Coordination chemistry for information acquisition and processing

Document Version:
Peer reviewed version

Queen's University Belfast - Research Portal:
Link to publication record in Queen's University Belfast Research Portal

Coordination chemistry for information acquisition and processing

Kacper Pilarczyk,[a,b] Brian Daly,[c] Agnieszka Podborska,[d] Przemysław Kwolek,[e] Victoria A. D. Silverson,[c] A. Prasanna de Silva,*[c] and Konrad Szaciłowski*[a]

[a] Academic Centre for Materials and Nanotechnology, AGH University of Science and Technology, al. MIckiewicza 30, 30-059 Kraków, Poland

[b] Faculty of Applied Physics and Computer Science, AGH University of Science and Technology, al. Mickiewicza 30, 30-059 Kraków, Poland

[c] School of Chemistry and Chemical Engineering, Queen's University, Belfast BT9 5AG, Northern Ireland

[d] Faculty of Non-Ferrous Metals, AGH University of Science and Technology, al. Mickiewicza 30, 30-059 Kraków, Poland

[e] Department of Materials Science, Rzeszow University of Technology, ul. W. Pola 2, 35-959 Rzeszów, Poland

* corresponding authors:

szacilow@agh.edu.pl, a.desilva@qub.ac.uk

Abstract: In the 21st century, information has become the most valuable resource that is available to modern societies. Thus, great efforts have been made to develop new information processing and storage techniques. Chemistry can offer a wide variety of computing paradigms that are closely related to the natural processes found in living organisms (e.g., in the nervous systems of animals). Moreover, these phenomena cannot be reproduced easily by solely using silicon-based technology. Other great advantages of molecular-scale systems include their simplicity and the diversity of interactions that occur among them. Thus, devices constructed using chemical entities may be programmed to deal with different information carriers (photons, electrons, ions, and molecules), possibly surpassing the capabilities of classic electronic circuits.

Introduction

This article reviews the development of research efforts on chemical information acquisition and processing made in Krakow and Belfast. Though starting from different positions and materials, there are conceptual parallels which have resulted in the construction of a common platform for systems of gradually increasing complexity operating on the ground of Boolean logic, fuzzy logic and other paradigms of higher complexity.[1] Indeed, two books have emerged from Krakow[2] and Belfast[3] which summarise chemical information gathering and processing research from around the world. This review develops the concepts presented there and in a chapter soon to be published in the book entitled "Advances in Unconventional Computing".

Semiconductors, molecules and light

Information processing is based on changes. If everything stays the same we do not get any message. The crucial factors which cause some changes in semiconductors and molecules are light, potentials and/or binding of atomic/molecular species. One of the most important characteristics of semiconductors and molecules is their ability to alter upon appropriate stimulation. Furthermore, many of these changes are reversible. Because light is the most powerful carrier of information, it is natural that photochemical and photophysical processes are recognized as the most suitable for information processing at the molecular scale. Semiconductors separate electron-hole pairs upon illumination within the appropriate wavelength range. This property is widely applied in photovoltaics, photocatalysis and in general photochemistry. It also allows the use of materials in semiconductor laser technology and optoelectronics, as well as in molecular photochemical industry. In terms of information processing, charge separation within molecularly-modified or unmodified semiconductors is embodied in the photoelectrochemical effect of photocurrent switching (PEPS), which can be applied in the construction of switches, logic gates and other basic elements used in computing systems. When molecules are considered alone, similar construction of switches, sensors and logic gates also becomes possible by modulating the competition between fluorescence and photoinduced electron transfer (PET).

In classical situations under illumination of n-type semiconductors anodic photocurrent is generated, whereas in the case of p-type semiconductors – cathodic photocurrent will be observed. However, in some special situations under appropriate polarization with external potential, a switching between anodic and cathodic photocurrent can be observed (Fig. 1).[4-7] This effect was described for the first time in literature in 2006

and since then it has been extensively investigated. This phenomenon is defined as the change in the photocurrent polarity due to the change in either the semiconducting electrode potential or/and the wavelength of incident light.[8] It was named the PEPS effect (acronym of PhotoElectrochemical Photocurrent Switching Effect).
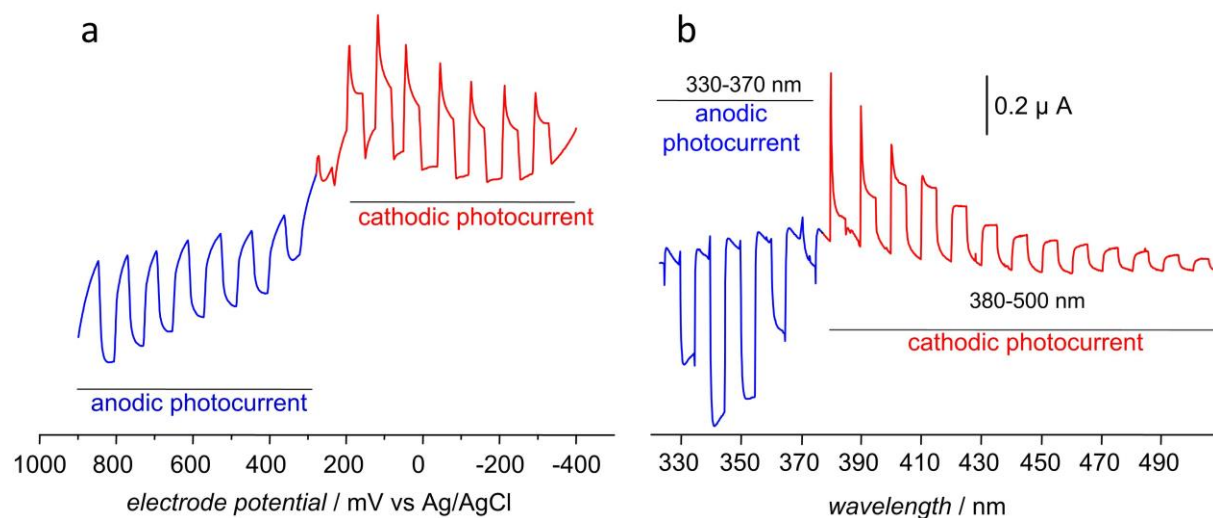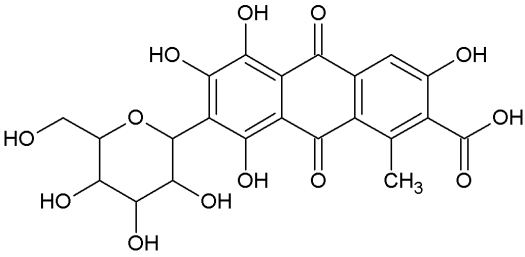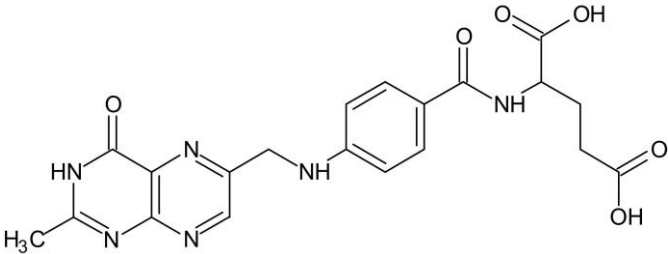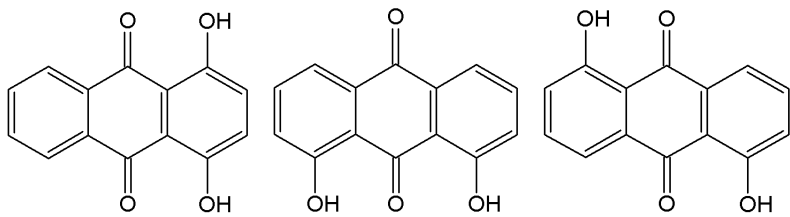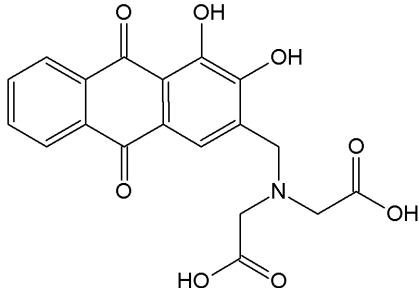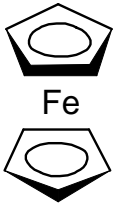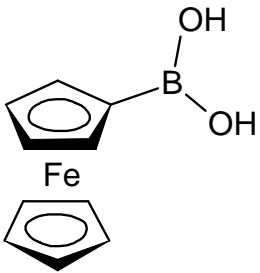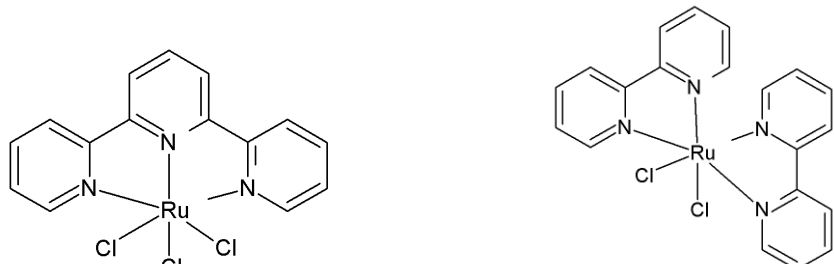

Fig. 1. A linear sweep voltammetry performed for n-type semiconductor (TiO_2 modified with $[Fe(CN)_6]^{4-}$) under pulsed illumination at 350 nm (a) and the photocurrent action spectrum of the same material recorded at 200 mV vs Ag/AgCl reference electrode with varying wavelength of the incident light (b)..

So far PEPS effect has been observed only for several groups of semiconducting materials. We can distinguish unmodified and surface-modified semiconductors. For the first group the photocurrent switching effect was observed mainly for unmodified oxide semiconductors such as bismuth orthovanadate,[30, 31] $Bi_xLa_{1-x}VO_4$ solid solutions (x between 0.23 and 0.93),[9] lead molybdate,[10] V-VI-VII semiconductors: bismuth oxyiodide,[7, 11] bismuth oxynitrate[12] and antimony sulfoiodide[13] as well as cadmium sulphide[14, 15] and lead sulphide.[16] For unmodified semiconductors, the observation of the switching effect is possible only for sufficiently low potential barrier E_{bi} at the solid-liquid junction – this may be achieved by the reduction in grain sizes of the semiconductor and the decrease in the doping level,[17] or when appropriate surface states are present.

More interesting examples are hybrid materials in which surface of semiconductor is modified with organic or inorganic species. Some most important examples of such materials are collected inTable 1.

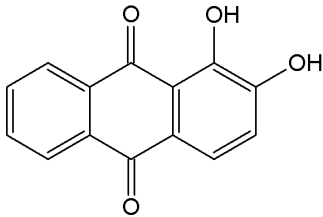Table 1. Molecular species reporter to induce photoelectrochemical photocurrent switching effect in wide band gap semiconductors.

semiconductor	modifier	ref
TiO$_2$	Carminic acid	18
TiO$_2$	Folic acid	19
TiO$_2$	hexacyanoferrate(II), $[Fe(CN)_6]^{4-}$	8, 20-22
TiO$_2$	pentacyanoferrates(II), L=H$_2$O, NH$_3$, thiamine, thiodiethanol, thiodipropanol, thiodiacetic acid, thiodipropionic acid, thiodipropionitrile, 1,3-dithiane, 1,3-dithiolene, thiamine	23, 24
TiO$_2$	Alizarin	25, 26

TiO$_2$	dihydroxyanthraquinones	25
TiO$_2$	alizarin complexone	27
TiO$_2$	Ferrocene	28
TiO$_2$	Ferroceneboronic acid	28
TiO$_2$	Prussian Blue	8, 29
TiO$_2$		30

TiO$_2$		31
TiO$_2$	CrO$_4^{2-}$, CrO$_3$F$^-$	32
CdS	Prussian Blue	8
CdS	Fullerene-oligothiophene 	33

When considering the examples presented in Table 1 we may formulate some general principles that must be met in order to observe the PEPS effect. The most obvious is the illumination of a semiconducting system within its absorption range in order to generate an electron-hole pair (except for the scenario in which a sensitisation of a semiconductor occurs). The second rule is the presence of efficient electron donors/acceptors dissolved in electrolyte, (for example: I$^-$/I$_3^-$,[11] Ce^{4+}/Ce^{3+},[10, 13] and sacrificial electron donors like EDTA).[34] This aspect influences both thermodynamics and kinetics of the system and should be considered at the design step for each device. The process is thermodynamically allowed when the redox potential of an electron donor/acceptor is located between the conduction and the valence band edges. Only in such a case, ΔG for the reduction of oxidized species from the electrolyte with an electron from the conduction band as well as the oxidation of reduced species with a hole from the valence band is negative. In our consideration we assume that the reduction

process is associated with the conduction band whereas the oxidation relies on the valence band.[35] Our assumption is usually valid when the band gap of a semiconductor is not too wide and for a relatively high reorganization energy value.

Considering the above cases, we can also note that the PEPS effect can be also observed in redox-innocent supporting electrolytes (*e.g.* aqueous solution of KNO_3), when the band gap of a semiconductor is sufficiently wide (more than ca. 2 eV).[9] In such a case, in the equilibrium with air, two redox couples – $OH^{\bullet}/OH^-$ and $O_2/O_2^{\bullet-}$ – can be distinguished. Their formal potentials are equal to 1.9 V[36] and −0.16 V vs. SHE respectively.[37] When the electrolyte is purged with oxygen, its reduction potential shifts anodically which facilitates cathodic photocurrent flow leading to the occurrence of the switching effect at sufficiently negative electrode potential.

The kinetic aspect of these processes is also crucial. The electron donor/acceptor system present in electrolyte should ensure the charge transfer through the semiconductor-liquid junction in a fast enough manner to avoid the recombination events. From the viewpoint of the thermodynamics, appropriate reduction potential values of the redox couples vs. the conduction and the valence band edges ensure the electrochemical stability of an investigated material. On the one hand, at sufficiently cathodic polarization of the electrode and in the absence of an efficient electron acceptor, the reduction of metal ions from the crystal lattice may occur. On the other hand, holes photogenerated under irradiation in the valence band may oxidize metal ions from the lattice. For oxide semiconductors it is usually not the case, however this problem has to be considered for sulphides and iodides.[35]
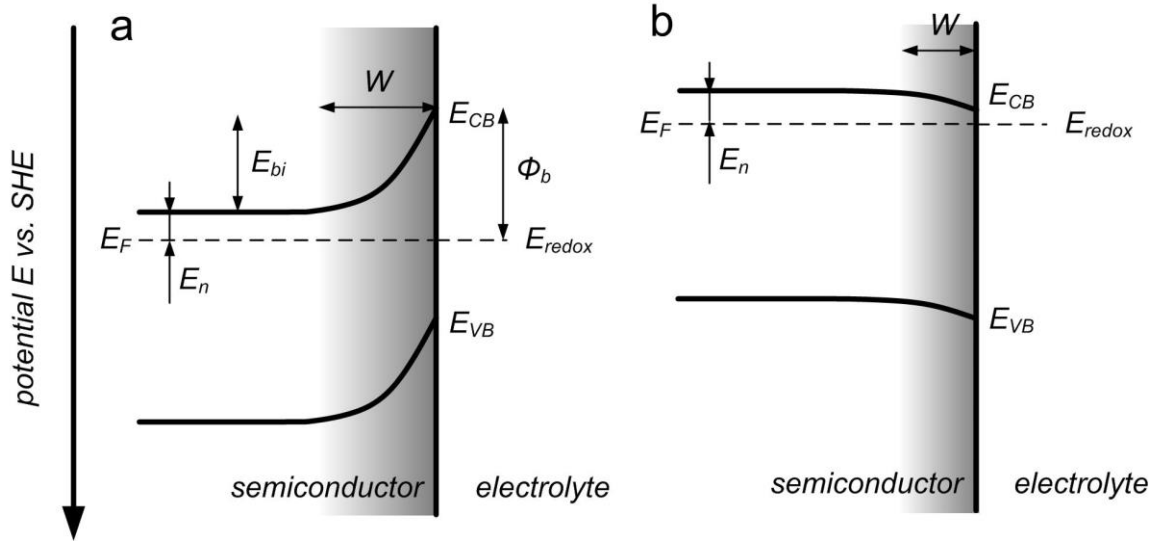
Fig. 2. The energy diagram for the n-type semiconductor-electrolyte junction at the equilibrium. The depletion layer (a) and the accumulation layer (b) are presented. The sign of the charge collected within the semiconductor part of the junction depends on the relative positions of the Fermi level E_F and the reduction potential of the redox couple E_{redox} in the electrolyte. E_{CB}, E_{VB} – the conduction and the valence band edge potentials, E_n – the Fermi level potential vs. E_{CB}, E_{bi} – the potential barrier at the junction, Φ_b – the potential difference between E_{CB} and E_{redox}, W – the depletion layer width.

Finally, the third factor having a significant impact on the occurrence and the mechanism of the PEPS effect is the potential barrier characteristics at the semiconductor-electrolyte interface. The stronger the electric field at the junction, the higher the intensity of anodic (and the lower the intensity of cathodic) photocurrents. In order to observe the switching effect, one should prepare a material with a moderate height of the potential barrier. Its value for a given system (of a defined size) may be tuned using two factors – the concentration of donor states and the space charge layer width according to the equation (1). The initial difference between Fermi levels of both counterparts in the junction is the driving force of the majority charge carrier flow. For the *n*-type semiconductor, the resulting depletion layer is usually 10 – 1000 nm wide (Fig. 2).[38] At the 1 V initial difference between Fermi levels, the strength of the electric field is around 10^5 V·cm^{-1}, which enables 1 μm separation of charge carriers from an electron-hole pair within picosecond timescale.[39] Since the potential distribution in the depletion layer is parabolic, the potential drop at the interface can be formulated as follows (1):[40]

$$\Delta\phi_0 = \frac{kT}{2e}\left(\frac{W}{L_D}\right)^2 \tag{1}$$

where e is the elementary charge, W is the depletion layer width and L_D is the Debye length (2). The Debye length is defined as follows:

$$L_D = \sqrt{\frac{\varepsilon kT}{eN_D}}, \tag{2}$$

where N_D is the concentration of electron donors. This description is valid for oxide semiconductors immersed in aqueous electrolyte in the dark.[35]

In the case of oxide materials, the concentration of electron donors in the lattice may be controlled during the annealing step in the oxygen-rich atmosphere. Lowering its partial pressure increases oxygen vacancies concentration, which are the most prominent electron donors in oxide semiconductors. On the contrary, high oxygen partial pressure decreases donor density and the potential barrier height at the solid-liquid interface. However, it should be noted here that it also decreases the electric conductivity of the electrode.[41] Alternatively, one may compensate a semiconductor by the implementation of acceptor levels within the energy gap (*e.g.* in the form of metal vacancies).[41,42] Semiconductor compensation via the introduction of defects into the lattice is believed to be responsible for the photocurrent switching effect observed in the case of $Bi_xLa_{1-x}VO_4$ solid solutions.[9] However, usually it is easier to control the width of the space charge layer. The thinner it is, the higher is the probability of the electron transfer from the conduction band to electrolyte to occur. The space charge layer width may be easily decreased by the reduction in semiconductor grain size. When the particle radius is significantly smaller than the estimated width of the space charge layer, equation (1) is not valid. In this case the potential drop at the interface is given by:

$$\Delta\phi_0 = \frac{kT}{6e}\left(\frac{r}{L_D}\right)^2 \tag{3}$$

Therefore for a sufficiently fine powder, the space charge layer is only partially developed resulting in a weak electric field at the interface. Yet, one must note that increasing cathodic photocurrent intensity concomitantly decreases anodic photocurrents. In the case of a small potential barrier, the relative photocurrent intensities depend mainly on the kinetics of the electron transfer from the conduction band to electron acceptors in electrolyte and the hole transfer from electron donors to the valence band.[43]

So far, the mechanism of the PEPS effect was usually described for the surface-modified, n-type semiconductors (mainly TiO_2, also CdS). To observe a significant signal from the organic or inorganic modifier adsorbed onto the oxide surface it is necessary to ensure as high a surface-to-volume ratio as possible. Thus, mainly nanoscopic semiconducting powders (*i.e.* with the diameter within the range of tens of nanometres) were investigated.[8, 14, 18-23, 28] In such cases, the variations in the space charge layer width can be neglected. The separation of electron-hole pairs depends mainly on the kinetics of the charge transfer through the solid-liquid junction. Upon the adsorption of a modifier onto semiconductor, in the dark, the equilibration of the Fermi levels is realized via the charge transfer through the interface. The current flow direction depends on the relative positions of the Fermi levels for electrons in the n-type semiconductor and the molecule of modifier. Since, usually very fine powder is subjected to the modification, the space charge layer is developed only to a small extent. Thus, the band bending may be neglected. In such a system there is a possibility to excite electrons in semiconductor from the valence to the conduction band, but also another processes involving surface molecules take place. These may include both electron transfer and hole transfer from the surface molecules, however the latter process is very rare,[44] therefore is not discussed in detail.

PET and OET processes

Electronic properties of hybrid materials depend on the interaction of both counterparts: semiconductor and organic/inorganic species.[45] The interaction between molecules and a semiconductor is based on a certain level of electronic coupling.[46] Depending on the strength of electronic coupling we can distinguish two kinds of processes which are involved in electron transfer in such a system: the optical electron transfer (OET) and the photoinduced electron transfer (PET). When the electronic coupling between molecule and surface of the semiconductor is strong OET dominates, whereas in the opposite situation PET is the winner. This can be explained on the basis of the Creutz-Brunschwig-Sutin model[47-50] for strong-coupled systems and by the Sakata-Hiramoto-Hashimoto model for weakly-coupled systems.[51, 52] Our preliminary computational results indicate that both models can be applied to describe higher catechol homologues adsorbed on titanium dioxide surfaces, depending on the number of fused aromatic rings and the structure of anchoring groups.[53-55]

When the electronic coupling between the molecule and the surface is strong enough, new surface coordination species and new energy levels are formed. The origin of which are the molecular levels of the ligands and the surface states of semiconductor counterpart. In the case of TiO_2, which is the *n*-type semiconductor, the interaction between HOMO level of the molecule (usually an aromatic π orbital) with empty surface states (titanium *d* orbitals) results in the formation of a bonding orbital. While the HOMO level of the system is mostly located at the molecule, the LUMO still belongs to the conduction band (Fig. 3a). When the excitation of a surface complex occurs, the optical electron transfer (OET) is observed *i.e.* an electron is promoted directly to the conduction band. It is possible in extreme situations, that *d* orbitals of only one Ti^{4+} ion may be involved in the optical electron transfer, followed by an ultrafast rearrangement of electronic structure and delocalization of electron over a large fragment of the lattice.[56, 57]

In the case of the weak electronic coupling, there is only one way of photosensitization which is called the photoinduced electron transfer (PET). Initially, when the photon with sufficient energy is absorbed, an electron is promoted from the HOMO to the LUMO of the system (Fig. 3b). In the case of conjugate aromatic photosensitizers (*e.g.* perylene, porphyrins, etc.) the ground state of the adsorbed molecule is its π-state, while the photoexcited state consists of π*-orbitals of the same aromatic system.[58] If the LUMO level is located above the conduction band edge, the electron transfer process is possible and an electron is injected into the conduction band to the energy level that is in resonance with the π* level.[59] Since non-exponential kinetics of this step was observed, it is possible, that the empty surface states, (probably unsaturated Ti^{4+} surface states with oxygen vacancies) may contribute to the photoinduced electron transfer.[60]

11
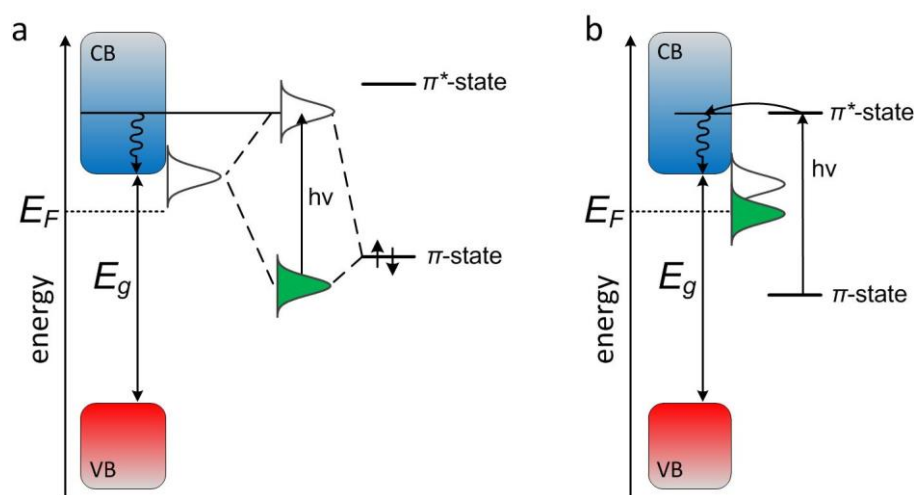
Fig. 3. The direct photosensitization of an n-type semiconductor according to the Creutz-Brunschwig-Sutin model (a) and the indirect photosensitization according to the Sakata-Hiramoto-Hashimoto model (b). White and green bell-shaped envelopes represent empty and occupied surface states respectively, E_F is the Fermi energy, E_g – the band gap, CB and VB stems for conduction and valence band respectively.

Depending on the local energetics and/or the electron transfer kinetics, electrons excited to the surface states/the conduction band may either reduce an electron acceptor in the electrolyte or be transferred to the conducting support. In this way cathodic or anodic photocurrents are generated, respectively. In most of the cases both processes take place simultaneously and the resulting photocurrent polarity is a result of the competition between them and depends on the wavelength of incident light (possibility of the excitation of both or only one counterpart of the hybrid material), the electrode potential and the interaction between semiconductor surface and an organic modifier. Possible electron pathways for a semiconductor-modifier system are summarized in Fig. 4.
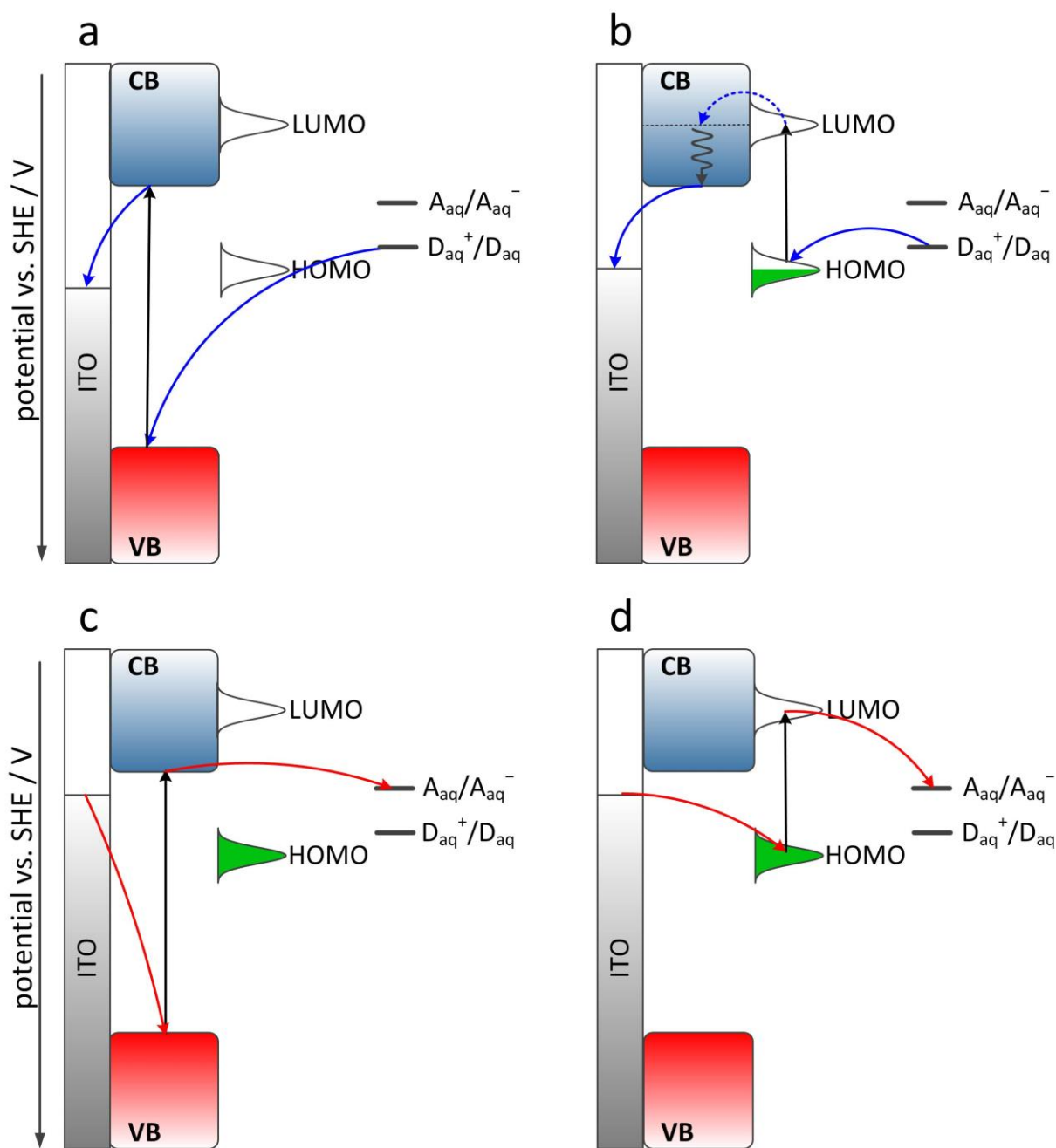
Fig. 4. Tentative mechanisms of the photocurrent switching for surface modified semiconductors, where HOMO and LUMO denotes highest occupied and lowest unoccupied molecular levels associated with the surface species: the photocurrent generation at semiconductor upon fundamental (a and c) and modifier (b and d) excitations at gradually decreasing photoelectrode potential. The anodic photocurrent generation at semiconductor upon fundamental (a) and modifier (b) excitations. The cathodic photocurrent generation at semiconductor upon fundamental (c) and modifier (d) excitations.

The simplest case, described in the previous section *i.e.* the anodic photocurrent generation occurring entirely within the semiconductor is presented in Fig. 4a. It may be observed for the wavelength range, in which the semiconductor is excited exclusively. The illumination within the absorption band of a modifier may also produce the anodic photocurrent (Fig. 4b), however the mechanism is more complicated and depends on the nature of the interaction between semiconductor surface and molecules. Depending on the strength of the electronic coupling of both counterparts there are two different possibilities for the electron transfer – the photoinduced electron transfer (PET) and the optical electron transfer (OET). The former is observed for weakly-coupled systems, whereas the latter – for strong interactions between a semiconductor and a modifier.

In the case of a weak electronic coupling, the photoinduced electron transfer is the only possible way of the photosensitization – both HOMO and LUMO levels of such a system are located mainly on the modifier (*e.g.* π and π^* states respectively for conjugate aromatic modifiers such as perylene and porphyrins).[58] The LUMO level of the system must be located at the lower potential than the conduction band edge. In such a case the electron injection to the conduction band may occur for the energy level in the resonance with the π^* level.[59] Subsequently, the injected electron moves towards the conductive substrate, whereas an electron donor from the electrolyte neutralizes the adsorbed molecule, provided that the redox potential of the electron donor is located between HOMO and LUMO levels. The most common examples of systems exhibiting PET are: TiO_2 – alizarin,[61, 62] TiO_2 – carminic acid[18] and TiO_2 – phthalic acid.[59]

In the case of a strong electronic coupling (like in a CT complex), new energy levels are formed from empty surface states of the semiconductor (*e.g. d*-states of titanium in the case of TiO_2) and HOMO levels of the ligand. Together they constitute a new LUMO level of the system, which mainly belongs to the conduction band, whereas the HOMO level is entirely located on the molecule. Upon the illumination, an electron is transferred between these two states and further, to the conductive substrate.[53] Subsequently, the oxidized ground state of the molecule is reduced with an electron from the electron donor present in the electrolyte. The OET has been observed for titanium dioxide modified with catechol[50, 58, 61] and salicylic acid.[63]

The electron injected into the conduction band should afterwards move inside the bulk material and through the relaxation move towards the band edge. The timescale of these two

processes is between one and two hundred femtoseconds. However, the recombination processes (involving both the chromophore and the sacrificial electron acceptor from electrolyte) are also possible, but these occur in the picosecond timescale – they are relatively slow as compared to the electron injection which takes place in hundreds of fs.[58]

Both, PET and OET processes may be observed when the redox potential of adsorbed species is located within the band gap of the semiconductor – it prevents modifier molecules from electrochemical degradation. Moreover, the electron transfer must occur at lower energy than the value of the band gap. Otherwise, the intense interband transitions will mask this effect.[50] In practice, the anodic photocurrent is often generated simultaneously via the molecule and the semiconductor excitation. The contributions of these two components in the net, measured photocurrent depend, among the others, on the number of adsorbed molecules, which in turn is proportional to the surface area of the semiconductor. For relatively big grains, the anodic photocurrent generated within the semiconductor is dominant.

The cathodic photocurrent is observed for sufficiently negative electrode potential. One may conclude that in this case two distinctive processes exist, namely the mechanism involving the semiconductor or the molecule which is excited. The former case was described in the previous section, where an electron from the conduction band directly reduces an electron acceptor from the electrolyte (Fig. 4c). In the latter case, the modifier excited state behaves as a very efficient electron donor which reduces the electron acceptor in the electrolyte, while an electron from the conductive substrate neutralizes the surface molecule (Fig. 4d). Such a behaviour has been observed for instance in the case of TiO_2-ferrocene[28] and TiO_2-cyanocarbons.[31]

For sufficiently big grains of semiconductor (or the material which is sufficiently highly-doped), the electron transfer from the conduction band to the electrolyte is very slow resulting in very low cathodic photocurrent intensity. On the other hand, the excitation of a modifier may result in a very intensive cathodic photocurrent generation. In such a way it is possible to induce the switching effect for hybrid materials, whereas it does not occur for the unmodified semiconductor. The presence of a potential barrier at the semiconductor-molecule interface arising from sufficiently coarse grains yields very interesting results, namely the anodic photocurrent is generated mainly in the semiconductor while the cathodic counterpart – in the molecules.

The described model may be further developed, if one takes into consideration that modifiers can undergo redox reactions within the experimental potential range – as *e.g.* in the case of TiO_2 modified with folic[19] and carminic acids.[18] In these situations the switching effect occurs only due to the polarization of an electrode. The most important hybrid materials, for which modifiers undergo redox reactions are TiO_2 nanoparticles modified with penta- and hexacyanoferrates.[20-24, 28, 64] For these systems, the photocurrent switching resulted either from the change in electrode potential or the wavelength of incident light. This phenomenon originated from different interactions between metal centres in Fe^{II}-C≡N-Ti^{IV} and Fe^{III}-C≡N-Ti^{IV} assemblies.

The anodic photocurrents in such systems are observed because of the semiconductor excitation provided that adsorbed molecules are oxidized. At sufficiently low potential (the surface species are reduced), the excitation of the surface complex within the MBCT band yields the cathodic photocurrent (an electron injected to the conduction band reduces the electron acceptor from the electrolyte). Still, the switching due to the wavelength change is possible at the potential value, where the modifier is only partially oxidized. Depending on the light wavelength either the semiconductor or the MBCT complex is excited leading to the generation of the anodic or the cathodic photocurrent respectively.

The last group of inorganic materials exhibiting the PEPS effect are bulk *p-n* heterojunctions. Also in this case it is possible to observe the switching effect due to the change of either the electrode polarization or the wavelength. Two conditions that must be met are: different band gap values of *p-* and *n*-type semiconductors(i) and an appropriate alignment of the band edges in the energetic scale(ii). The former enables the selective excitation of only one counterpart of the junction, the latter prevents the parasitic electron transfer between particles of different conductivity types. If these two prerequisites are not fulfilled, only one photocurrent direction will be preferred and no switching effect will be observed.[17]. The most significant examples of the switching effect observed for *p-n* heterojunctions are: $n - TiO_2 - N/p - CuI$,[34] $n- BiVO_4/p - Co_3O_4$,[65] $n - TiO_2/p - Se$,[4, 5] $n - CdS/p - CdTe$,[66] $p - PbMoO_4/n - Bi_2O_3$[67] and p-CuO/n-$CuWO_4$.[68]

A similar behaviour can be observed also in the case of inorganic *n*-type semiconductors modified with organic semiconductors. Nonetheless, only few such materials have been reported so far: titanium dioxide/ferrocene,[28] titanium

dioxide/hexacyanobutanedienide,[31] titanium dioxide/hexacyanodiazahexadienide[31] and cadmium sulphide/fullerene-oligothiophene[33] systems.

Photoelectrochemical properties of fullerene-modified CdS are very different from unmodified material. In the absence of dissolved oxygen, however it behaves much the same as the untreated CdS and photocurrent switching cannot be observed. In the presence of dissolved oxygen, however, the photoelectrical characteristics of fullerene-modified CdS change dramatically. When photoelectrode is positively polarized usual anodic photocurrents are observed, but upon negative polarization cathodic photocurrents are generated (Fig. 5a).

The transition between the anodic and cathodic regimes is sharp and wavelength-independent, which contrasts the typical photocurrent switching characteristics recorded for other systems exhibiting the PEPS effect.[22, 23] It indicates that the photocurrent is generated solely by the inorganic counterpart, whereas the fullerene-based modifier influences only the fate of the conduction band electrons. At sufficiently high photoelectrode potentials electron transfer from the conduction band through the Schottky barrier to the conducting support is the most favoured process. With decreasing photoelectrode potential this process is less favoured and the alternative pathway becomes dominant: electrons from the conduction band are collected by the surface-deposited fullerene moieties, with thiophene moieties facilitating the fullerene-CdS interactions. Thus, generated fulleride anions are sufficiently good electron donors to reduce molecular oxygen dissolved in the electrolyte. Reduction of molecular oxygen is further facilitated by the hydrophobic nature of fullerene derivatives.[28] Depending on the number of thiophene units the switching potential can be tuned within the range of $-0.15 \div -0.25$ V, which is associated with variation of the first reduction potential of thiophene-fullerene conjugates. This clear dependence supports the photocurrent switching mechanism described above and shown in Fig. 5 b-c. Anodic photocurrents are generated according to well-established mechanism involving charge separation, followed by electrons scavenged by the conducting support and holes oxidizing the redox mediator in solution. At more negative polarization of the photoelectrode molecular oxygen is being reduced at the surface of the photoelectrode. This process is mediated by fullerene-based modifier, which also can act as an oxygen concentrator due to its hydrophobic character.
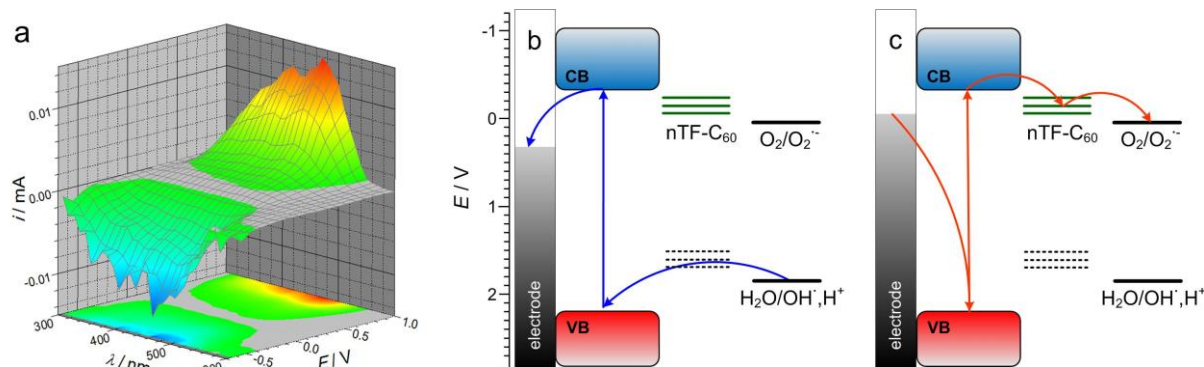
Fig. 5. Photocurrent action spectra recorded as a function of photoelectrode potential for CdS modified with fullerene-thiophene conjugate (cf. Table 1) in the presence of oxygen dissolved in the electrolyte (a). The mechanism of anodic (b) and cathodic (c) photocurrent generation at CdS modified with thiophene derivatives. Adapted from Ref. 33.

In the absence of semiconductors, the situation is simpler since PET rather than OET rules under most conditions. However the molecules themselves need to carry some level of complexity in order for information gathering and processing tasks to be achieved. This is done by building molecules according to the 'fluorophore-spacer-receptor' format[69, 70] so that photonic and chemical transactions are both enabled.

When light is absorbed by a fluorophore, an electron is caused to move from the HOMO to the LUMO. This excited state is unstable and falls back to the ground state emitting the excess energy as a new photon which may be observed as fluorescence. However if another MO is in close proximity, and possesses the correct energy and symmetry, it can cause a diversion. This HOMO' can transfer an electron to the HOMO of the fluorophore. This exergonic transfer (PET) fills the HOMO and prevents the excited fluorophore from falling back to ground state and the result is the absence of an emitted photon. If the properties of this HOMO' can be manipulated then the two competing processes of fluorescence and PET can be controlled.

Let us consider a HOMO' that is derived from a tertiary amine receptor as an example. The lone pair of this amine can form a dative covalent bond to H^+. The emergence of this new N-H σ bond transforms the HOMO' to the HOMO'' at such an energy level where it can no longer interfere. Fluorescence is only visible when the amine is protonated so the emission of a photon acts as a reporter for the state of the amine and simultaneously as a reporter for H^+.

Further analysis shows that pH values around the pK_a value of the amine receptor can be accurately measured by the 'fluorophore-spacer-amine' system, i.e. it acts as a pH sensor.[69, 71] Importantly the combination of these receptors and fluorophores has little effect on their properties (except for the switching of fluorescence) in favourable instances. The binding constants of the receptor are virtually identical whether or not it is combined with the 'spacer-fluorophore' components.[72, 73] This means that such molecular devices can be built in an 'off-the-shelf' fashion. Components are chosen for their intrinsic properties and these remain virtually unchanged as the molecular superstructures are built.
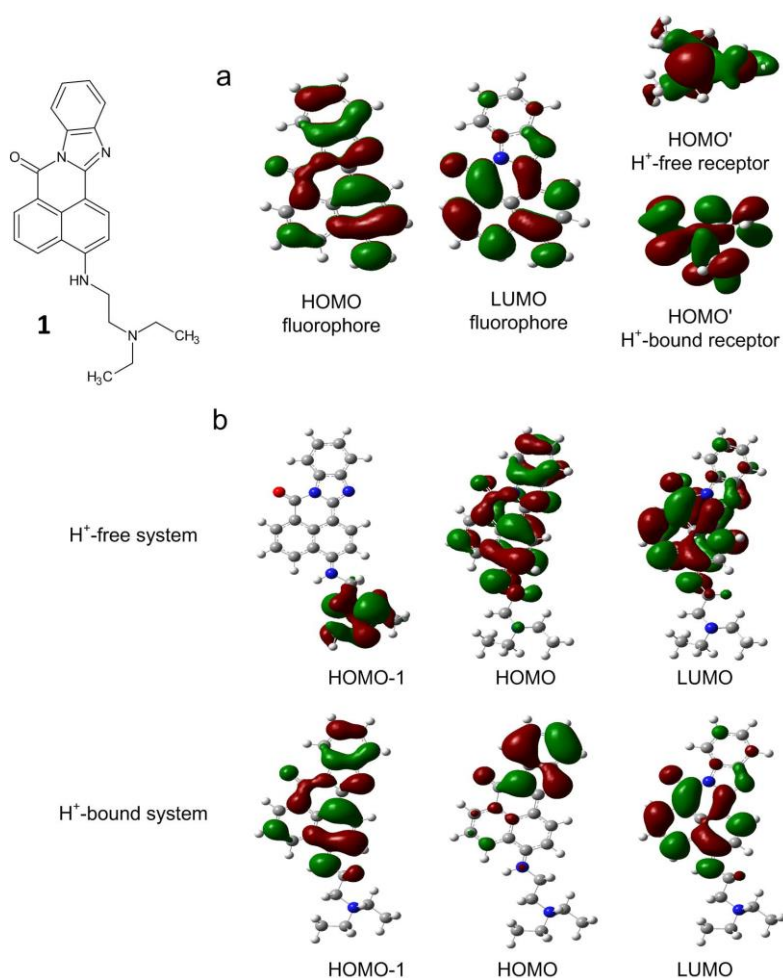
Fig. 6. The molecular structure of 1[74] and the frontier orbitals of (a) its components and of (b) the superstructure, without and with H^+. In the part (a), the energies of the HOMO, LUMO, HOMO' and HOMO'' are estimated (DFT-B3LYP) at -7.9, -5.7, -5.3 and -11.6 eV respectively. We notice that the energy of HOMO' of the receptor will adjust to a value of lower than -5.7 eV if the presence of an electron withdrawing group across the spacer is allowed.

The chemically-switchable competition between fluorescence and PET, which was outlined in the previous paragraph can be put on a more quantitative footing by resorting to quantum theoretical calculations.[75-83] The extreme convenience with which these can be performed nowadays can be illustrated by the approximate evaluation[84] of **1**, a member[74] of the Lysosensor Green™ series,[85] which is sold for visualization of acidic compartments in living cells where ingested food is digested. Fig. 6a shows the HOMO of the fluorophore and the HOMO' of the H^+-free receptor components separately, among other things. The energy difference between them makes PET exergonic, In general, the 0.1 eV of ion-pairing energy present within the resulting radical ion pair[86] should also be taken into account. On the other hand, the HOMO'' energy of the H^+-bound receptor is so low that PET is severely endergonic and therefore fluorescence is the result. Fig. 6b shows the HOMO-1 of the 'fluorophore-spacer-receptor' system, when it is free of H^+, localized on the receptor. This orbital is close – in terms of energy – to the HOMO and hence would couple with it. Since the LUMO is localized on the fluorophore, HOMO-LUMO excitation results in the electron essentially transiting from the receptor to the fluorophore. In contrast, the H^+-bound version shows both the HOMO and LUMO to be restricted to the fluorophore. Thus the excitation and de-excitation involve the fluorophore only, along the photonic channel.

Information gathering with molecular 'fluorophore-spacer-receptor' systems

Humans have boldly gone beyond the confines of our planet. This is possible because space, cold and inhospitable as it is, is vast. When we encapsulate ourselves in a Soyuz rocket and are delivered to the international space station, space remains essentially unperturbed. The vastness and emptiness means that our presence has almost no effect on its dynamics. There are however some areas of interest to which we may never travel. This is not through lack of ingenuity or desire but because these spaces are not only smaller than us but in many cases the spaces are inside of us. To investigate the properties of these spaces we must follow our colleagues that examine the cosmos and send a probe. However these small spaces pose unique challenges. Not only must the probe fit within the space of interest but it must also function as a reporter. Its presence must leave the normal dynamics of the space virtually unperturbed. So how can we develop a miniaturized Philae lander that can examine without digging? We must use molecules because of their smallness, which allows them access to interesting nano-, micro- and millimetric spaces. Molecular reporters are therefore capable of

sending us intelligence from these domains where humans are barred. Many of these domains are physiologically crucial and therefore issues concerning human health and illness can be profitably addressed in this way.

Some of the most easily prepared nanospaces occur in aqueous solutions of detergents, where spherical micelles are formed.[87] These, and their associated counterion clouds, have radii of a few nanometers. Although they are simple, they can serve as models for investigating membrane-bounded ions and membrane-bounded water. For instance, membrane-bounded H^+ determines general bioenergetics and membrane-bounded Na^+ underpins nerve signals.[88] Suitably targeted fluorescent PET sensors[89] can report on membrane-bounded H^+ and advanced versions[90] can even map H^+ in these nano-environments as shown below.

The mapping is achieved with a multiplexing fluorescent sensor **2[90]** which simultaneously monitors multiple environmental parameters by means of multiple emission properties.[91] The distribution of H^+ can be mapped by simultaneously collecting information on both the H^+ density observed by the sensor and the sensor position. H^+ density in a localized position in aqueous solution can be measured using a simple fluorescent pH sensor like **1**,[74] after appropriate calibration for the micellar medium.[92] A multiplexing fluorescent sensor like **2** can do the same. The position can be determined when the change in polarity across a micelle is considered. On traveling outwards from the centre of a micelle along a radial line the environment changes from that of the hydrophobic alkane chains to that of the hydrophilic head groups. If local polarity is measured along this line it would initially correspond to that of alkanes and would eventually correspond to that of bulk water. As the head groups are passed, bound water molecules would become apparent to us as the polarity value will be significantly reduced when compared to that of bulk water. The internal charge transfer (ICT) excited state of sensor **2** allows it to measure local polarity by means of emission wavelength shifts[93] which can be translated as a location with respect to the centre of a micelle. Since the H^+ density is measured simultaneously, the multiplexing sensor **2** produces a data pair of H^+ density and location. By using many sensors scattered over different positions of the aqueous micelle, by virtue of their individual hydrophobicities, a nanoscaled mapping of H^+ density can be achieved (Fig. 7).
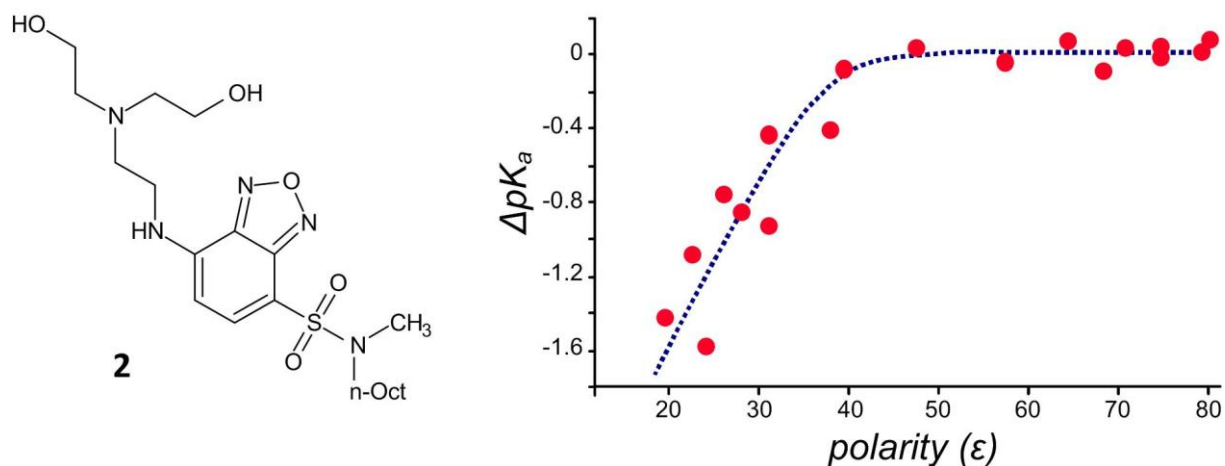
*Fig. 7. The molecular structure of **2**[90] and the map of H$^+$ density in an aqueous charge-neutral micellar system.*

As alluded to above, **2** contains an ICT fluorophore, though within a 'gross targeting unit-fluorophore-spacer-receptor-fine targeting unit' system. The gross and fine targeting units on either end hold the sensor close to the charge-neutral micelle while moving the lumophore and receptor to a characteristic location. Fig. 7 gives the position of a series of derivatives of **2** in terms of local polarity as measured by the mean dielectric constant. The ordinate gives the local H$^+$ density measured by the pK$_a$ shift in the micellar medium compared to bulk water. It can be seen in Fig. 7 that H$^+$ density increases with an increasing distance from the centre of the micelle. The H$^+$ density is seen to level off as polarity comes closer to that of bulk water farther away from the head groups. This graph is proof that ions are repelled away from the relatively apolar membrane toward bulk water and provides a quantitation of the effect.

*Fig. 8. The molecular structures of Na$^+$ sensors **3**-**4**,[94] control compounds **5**-**8**[94] and fluorescence spectra of **3** (excited at 376 nm) as a function of bulk Na$^+$ concentration in an aqueous anionic micellar system.*
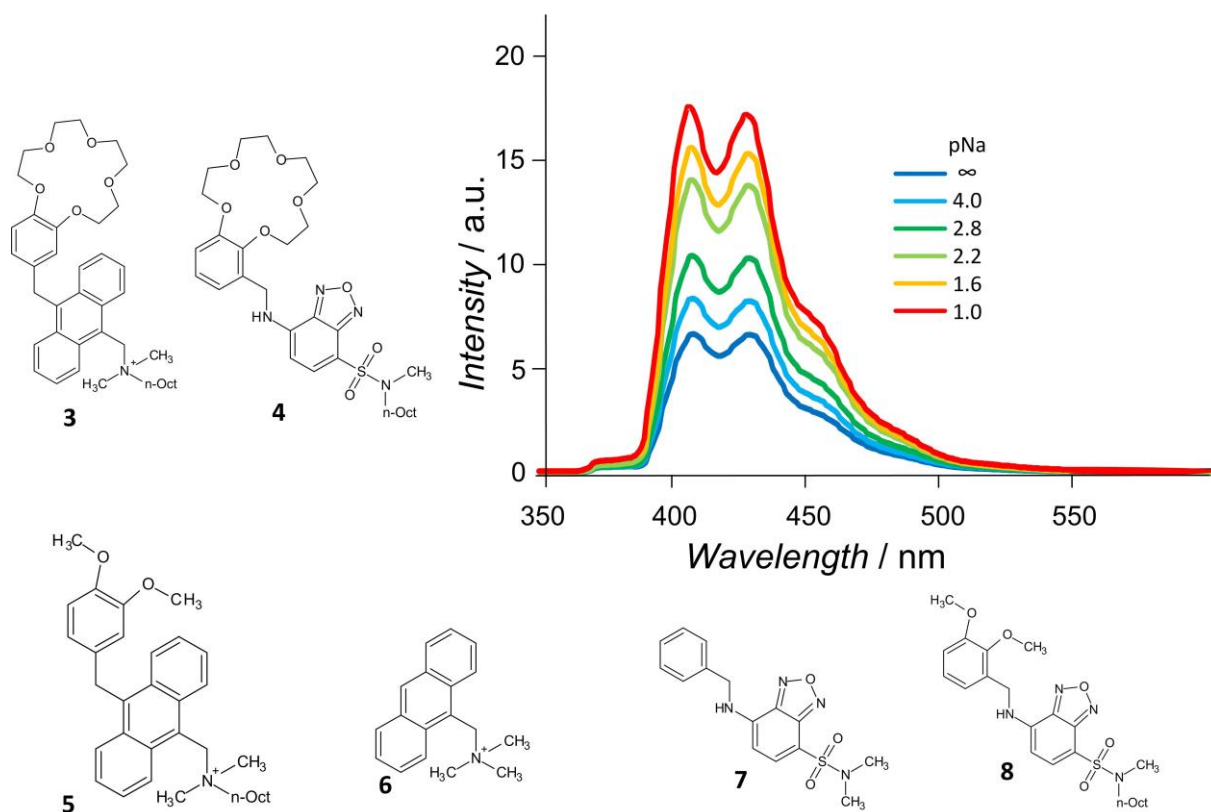
The concept of measuring ion densities near micellar membranes can be developed to include Na$^+$.[94] The format of 'gross targeting unit-fluorophore-spacer-receptor' is used in this instance. The receptor is of particular importance as it must be selective for Na$^+$ against H$^+$ to the point where it is virtually insensitive to H$^+$. This is because some unexplored membrane-bounded nanospaces could have highly amplified H$^+$ densities large enough to interfere with the correct functioning of Na$^+$ sensors which have a finite response towards H$^+$. For this reason a benzo-15-crown-5 ether,[95] which only binds H$^+$ under extreme acidities, is chosen. Two different fluorophores are chosen, anthracene and a push-pull benzofurazan, within **3** and **4** respectively. Both are hydrophobic which targets them to micelles[94] and both take part in PET processes with benzo-15-crown-5 when vacant,[96] emitting strong fluorescence when Na$^+$ is captured (Fig. 8). The emission of the push-pull benzofurazan has the added advantage of being polarity sensitive due to its ICT excited state as hypsochromic shifts are observed in a hydrophobic environment.[97] Two control compounds, which are unable to bind Na$^+$, are

used for each sensor. One of these compounds, (**5/8**) always has PET (fluorescence 'off') and the other (**6/7**) has no PET channel (fluorescence 'on'). These control molecules, especially the ones carrying the PET channel, warn against any extremely apolar micelle nanoenvironments, which can produce a false positive in the Na^+ sensors. Fluorescence switching 'on' is only observed for anionic micelles where electrostatic attraction between its head-groups and the cationic sensors holds the latter right next to the micellar surface. The electrostatic attraction also causes Na^+ to be concentrated in the same place to such an extent that the benzo-15-crown-5 receptor can be extensively occupied. In the best case, Na^+ is found to be concentrated by a factor of 160.

The use of fluorescent PET sensors to map chemical species in micrometric environments is well-established and well-reviewed.[98] Indeed, much physiology has been illuminated in exactly this way. For instance, **1**'s capability to visualize acidic compartments of living cells has been mentioned already. Far more important examples are available[99] which visualize Ca^{2+} waves as the language of internal cellular communication.

While the ability of a sensor molecule to roam free in homogeneous solution leads to fertile applications in intracellular regimes,[100] solid-bound sensors are robust enough to be used outside of research laboratories in the form of devices with millimetric internal dimensions. The latter means use at the hospital bedside, in the battlefield, or even on the street. To be of use to a health practitioner, a Na^+ sensor must be effective around 0.15 M Na^+ - the level found in normal blood. Its effectiveness is governed by the binding constant (β_{Na+}) which must have a value of around 6. This is where the predictive power of modular fluorescent PET systems can be exploited. The binding constant of the receptor is unchanged by construction of a spacer between it and the fluorophore. This means that one may need only to search literature for a Na^+ receptor with the correct properties and suitable lariat ethers were found.[101] The fluorophore which communicates the Na^+ binding cannot function in the ultraviolet region, as even with blood filtering the remaining serum cannot transmit light in this region. The 4-aminonaphthalimide fluorophore has suitable properties and is an inexpensive commodity chemical which can be excited by cost-effective blue light-emitting-diodes. The dimethylene spacer allows PET at sufficient rates to ensure that **9** would function as an 'off-on' fluorescent sensor for Na^+.[102] The system is immobilized on aminocellulose fibres with a sufficiently long linker to minimize perturbation of the sensor properties. Similar 'off-on' sensors for K^+ and Ca^{2+} are constructed by altering the receptor component of **9**. These sensors together with others for pH, P_{CO2}, P_{O2} and Cl^- are mounted into a single cassette

(Fig. 9) to form the business end of the OPTI blood gas and electrolyte analysers.[103] The OPTI system requires 120 µL of whole blood and performs the measurement in around 30 seconds. The measuring device is convenient and requires little training for its use. In social terms, the speed and portability of the device has undoubtedly saved lives. In economic terms, the use of OPTI technology by the healthcare and veterinary professions worldwide has generated around 530M $ for the measuring device alone.
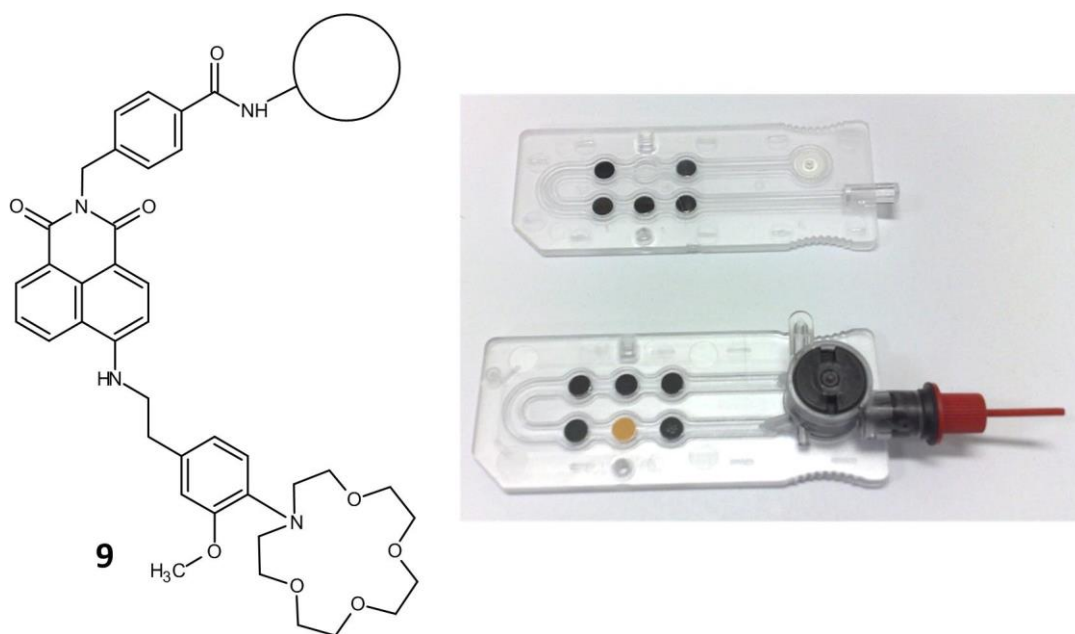
Fig. 9. The molecular structure of Na⁺ sensor 9^{102} and the OPTI blood diagnostic devices. Photograph adapted from ref. 73.

Boolean logic devices based on the PEPS effect and on other molecular phenomena

Although Boolean logic devices underpin modern semiconductor-based computers,[104, 105] experiments with molecules to perform Boolean logic operations are only 22 years old.[106] Though these experiments concerned molecules free in solution now the studies have diversified to include molecules adsorbed on solids. It is also important to note that the cases discussed in the previous section can be understood as single input-single output YES logic gates. The present section will consider more of these gates, as well as those of a more complex nature.

Since the PEPS effect allows the straightforward control on the photocurrent polarity via two independent channels (*i.e.* the wavelength of incident light and the photoelectrode

potential), materials exhibiting this effect are suitable for the construction of Boolean logic gates. In most of the cases it is sufficient to assign appropriate Boolean values (0 and 1) to the specific ranges of the input stimuli and to the output states. In more complex systems, two different wavelengths can be used as the inputs and the generated photocurrent can be interpreted as the output. The most convenient material for light-only control is titanium dioxide modified with hexacyanoferrate(II) anions. The surface interactions lead to the formation of cyanobridged, two-dimensional assembly with Fe-C≡N-Ti bonding framework.

In an original experiment two LEDs (with wavelengths equal to 400 and 460 nm) were used as the light sources. Boolean 0 and 1 states were assigned to off and on states of each diode playing the role of two independent inputs. At the exit, the Boolean 0 was assigned to null net photocurrent, while any nonzero photocurrent intensity was interpreted as the Boolean 1 (irrespectively of its polarity). During the pulsed irradiation with the violet diode (400 nm) at the potentials that oxidize completely the surface species (+400 mV vs Ag/AgCl reference electrode), the anodic photocurrent is generated and the irradiation with the blue LED (460 nm) does not give any signal. The synchronized irradiation with both diodes lead to the same effect as the use of the violet diode alone (Fig. 7, Table 1, output 1).[21, 22]
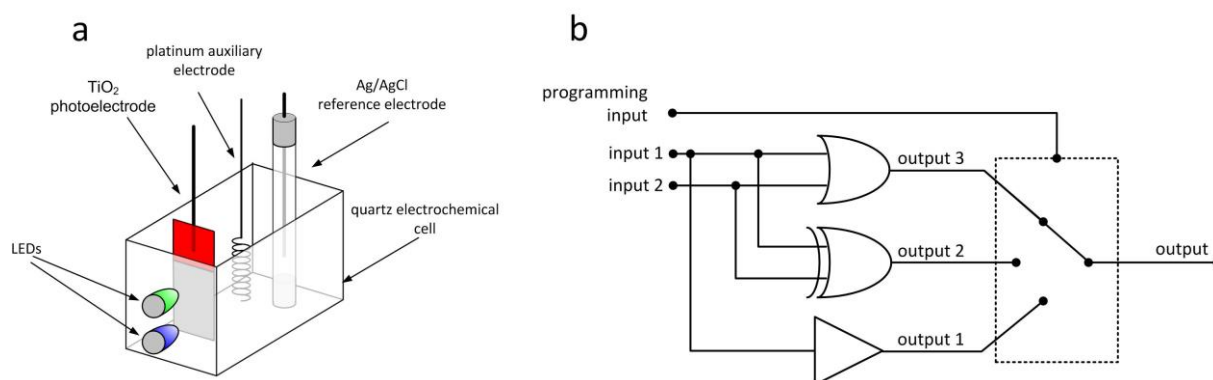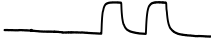
Fig. 10. The experimental setup for the measurement of a reconfigurable logic device prototype (a) and an electronic equivalent circuit for the logic system based on a modified titanium dioxide electrode (b). Output 1 follows the input 1 signal, output 2 computes the XOR function of input data while output 3 corresponds to the logic sum (OR) of input data. The three-position switch represents the programming functionality of the device through the photoelectrode potential. Adapted from Ref. 21.

At the lower potentials the electrochemical reduction of surface species takes place. The irradiation of this material with violet and blue diodes leads to the generation of cathodic

photocurrent. Simultaneous irradiation by both LEDs effects in photocurrent of much higher intensity. This kind of behaviour of the photoelectrode at -200 mV vs. Ag/AgCl corresponds to the OR logic gate operation (Fig. 10 Table 2, output 3). The partial oxidation of the surface complex results in yet another observation. The violet light pulses generate the anodic photocurrent, which is consistent with the excitation of an inner part of semiconductor particles. The blue light pulses generate the cathodic photocurrent and the synchronized irradiation with both LEDs gives null net current as the anodic and the cathodic photocurrents compensate effectively (Fig. 10, Table 2, output 2). It corresponds to the XOR gate function. This system represents the first example of the photoelectrochemical XOR logic gate with two optical inputs.

Furthermore, the system is reconfigurable and its logic characteristics can be changed via an appropriate polarization of the photoelectrode.[22, 107] The rich chemistry of cyanoferrate complexes combined with the reactivity of wide band gap semiconductors creates numerous possibilities for other, even more complex logic circuits based on simple chemical systems. The information is supplied to the device through the pulses of light, is processed by the electrochemical interactions and retrieved in the form of current spikes. This behaviour allows facile communication between various electronic components and chemical logic systems.[21-23]

Table 2. The truth table for logic gates based on $[Fe(CN)_6]^{4-}$ modified titanium dioxide photoelectrodes. Adapted from Refs. 22, 107.

input 1	input 2	output		
400 nm	460 nm	400 mV	250 mV	−200 mV
0	0	0	0	0
0	1	0	1	1
1	0	1	1	1
1	1	1	0	1
Boolean function		YES	XOR	OR

Similar, albeit more simplistic behaviour was observed for titanium dioxide modified with pentacyanofferrate(II) complex of thiamine,[24] folic acid,[19] and carminic acid.[108] Thiamine itself cannot bind to the surface of titanium dioxide and it requires an additional

anchoring group. It can be bound to the surface of nanocrystalline titania via a pentacyanoferrate linker. Materials obtained by the immobilization of these chromophores onto the surface of TiO_2 behave similarly to those obtained via the deposition of redox-active cyanoferrate complexes. This is possible because of organic chromophores containing π-electron systems that can act here as electron buffers, donating or accepting electrons if necessary.[109] In principle, any electrochemically active, amphoteric molecule with its energy levels properly aligned with the semiconductor bands[110] should yield an optoelectronic switch.[64, 111] It seems easy, but it is a nontrivial task, as the molecule must be photostable and should be resistant to the photocatalytic degradation in the contact with semiconducting surfaces.[112, 113]

The PEPS effect allows the use of such systems as optoelectronic two-channel demultiplexers (Table 3). In this case it is also possible to assign the logic values to input and output signals for the logic operation analysis. '0' value can be related to the negative polarization and '1' value to the positive polarization of a photoelectrode. In the case of the optical input the simplest and the most natural signal assignment is achieved when the logical '0' and the logical '1' correspond to the light turned off and on respectively. In the case of photocurrent switching, when both polarities of photocurrent are allowed, it is convenient to split the electric output into two channels, one associated with the anodic photocurrent, and the other with the cathodic one. The photoelectrochemical system defined this way follows the behaviour of the 1:2 demultiplexer (Fig. 11).

Table 3. The truth table for the 1:2 demultiplexer. Adapted from Refs. 19, 107.

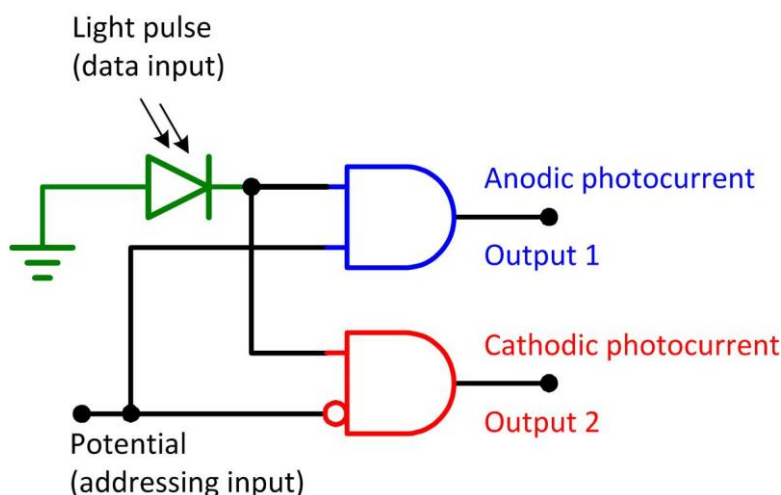| light	input 1	photoelectrode potential	input 2	photocurrent	output 1	output 2
OFF	0	positive	0	NO	0	0
ON	1	positive	0	cathodic	1	0
OFF	0	negative	1	NO	0	0
ON	1	negative	1	anodic	0	1

Fig. 11. The electronic-equivalent circuit of a photoelectrode based on wide band gap semiconductors (TiO₂, CdS) modified with redox active species.

An interesting example of a single nanoparticle which could be used in the construction of an optoelectronic 1:2 demultiplexer is provided by nanocrystalline S-doped CdS.[114] The photoelectrode made of sulphur-doped cadmium sulphide generates the anodic and/or the cathodic photocurrents depending on the incident light wavelength or the applied bias. This unexpected behaviour of nonstoichiometric CdS was attributed to the presence of additional sulphur atoms which results in the existence of additional energy levels within the band gap.[14] Under the potential higher than the conduction band edge potential the anodic photocurrent, which is characteristic for CdS, was observed. However, when the potential has been lowered beyond the potential of the sulphur-associated doping states only the cathodic photocurrent was recorded. The polarity of the generated photocurrent depends also on the incident light wavelength. The illumination with light of higher energy results in anodic photocurrent – the excitation within fundamental transition occurs – whereas lowering the energy results in the cathodic photocurrent generation associated with the valence band to sulphur-centred gap states transition.

The peculiar photoelectrochemical behaviour of S-doped CdS nanoparticles of 5-7 nm in diameter can be used to build the 1:2 demultiplexer operating on the same principle as in the case of surface-modified titanium dioxide. Interestingly, all the switching phenomena occur at the single nanoparticle level and do not require any cooperative interactions between nanoparticles. Despite the fact, that the operation of these systems has been demonstrated only

on a large set of nanoparticles, similar devices have been reported to work at a single nanowire level.[115-118]

The photoelectrochemical properties of nanoparticulate CdS deposited on conducting substrates open the way for the construction of nanoscale photoelectrochemical arithmetic systems. The optoelectronic binary half-adder can be built from nanoparticle-based ITO/CdS Schottky junctions working in iodide-loaded, semi-solid ionic liquid electrolyte.[119] The single Schottky junction was made by the chemical bath deposition of thin layer of CdS on the ITO surface or by the cast-coating onto the conductive support with thiourea-capped CdS nanoparticles. At no external bias the illumination of the junction results in the anodic photocurrent generation. The combination of two Schottky photodiodes with identical polarities results in the operation resembling AND logic gate as the high intensity photocurrent can be recorded only upon the illumination of both junctions. The opposite polarization of photodiodes naturally leads to the XOR gate, as the illumination of any single junction generates certain net photocurrent, while the concomitant illumination of both junctions results in the compensation of photocurrents.

An appropriate concatenation of these two optoelectronic systems leads to the construction of an optoelectronic binary half-adder. In this device two input signals (light pulses) generate current pulses in two different circuits (corresponding to the AND and the XOR logic gates) and thus yield the binary representation of the sum of the input signals.[119] These devices, similarly to the previously described, do not require any interactions between individual particles and therefore the whole arithmetic unit can be confined within the size of two small nanoparticles.

The described materials give the possibility for the photocurrent direction control through both stimuli: the change in the wavelength or the photoelectrode potential. These structures are not composites comprising of two types of semiconductors but are engineered as uniform materials and the photocurrent switching phenomenon is their intrinsic feature resulting from a specific electronic structure of the system. In this sense the materials described in this chapter are unique. The PEPS effect may serve as a basis for the construction of tunable, light-harvesting antennae, chemical switches, logic gates, and many other optoelectronic devices.

Just like logic gates arose from the PEPS effect concerning semiconductors with/without molecular modifiers, it is possible to develop logic gates from molecules alone.

Our early examples of this type concern chemical inputs and fluorescence outputs.[106, 120-125,127] Here, we discuss a three-input AND logic gate[126] to illustrate medical applications of molecular logic-based computation.

The medical profession aids and facilitates our recovery from disease or illness through examination. More often than not this examination is chemical as well as physical. Diseases prevent our bodies from functioning normally and either as a cause or consequence of this malfunction the chemical make-up of our cells and bodily fluids change. Whilst such biofluid screening is commonplace in hospitals, the process can involve dozens of people and require sample transport to a clinical laboratory. Laboratory equipment is large, expensive and requires a trained technician to operate it. There are instances (in theatres of war, in less developed countries and during times of civic strife or pandemics) where such laboraory systems are not available or are overloaded. There are other instances, e.g. in critical care wards, where the process of engaging the clinical laboratory is too slow. However, the development of a 'lab-on-a-molecule' would give us a portable device that can draw medical inferences from a Boolean logical combination of how a set of analytes deviate from their normal values. A detailed measurement of the analytes is not required. We develop such a case,[126] **10** (Fig. 12) which examines the levels of Na^+, H^+, and Zn^{2+} simultaneously and gives a strong fluorescence signal only when the levels of each are simultaneously determined to be 'high' when compared to normal values.

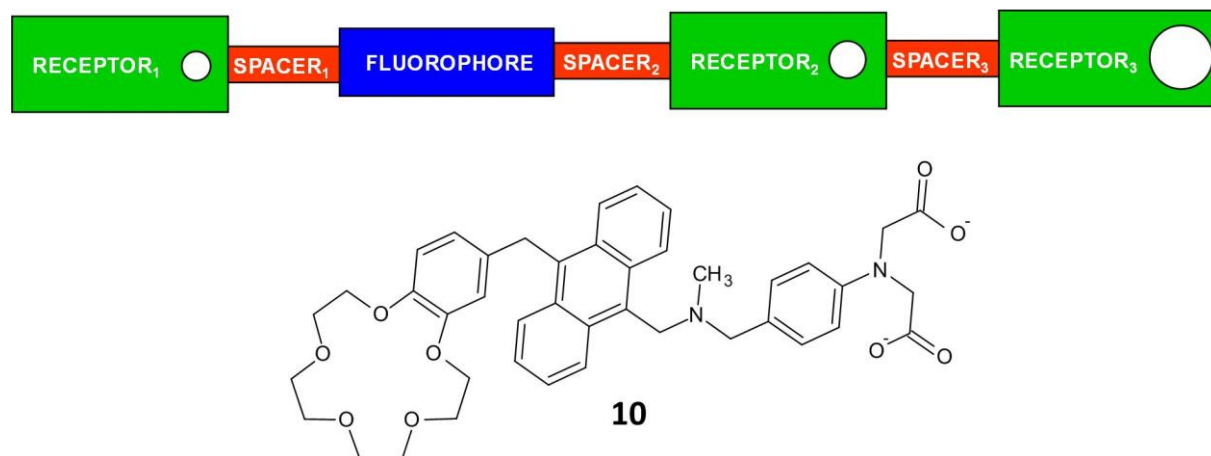*Fig. 12. The molecular structure of 'lab-on-a-molecule' **10**[126] and its modular construction.*

The diagnostic molecule in question is built according to the 'receptor$_1$-spacer$_1$-fluorophore-spacer$_2$-receptor$_2$-spacer$_3$-receptor$_3$' format. The benzo-15-crown-5 ether receptor binds Na^+, the tertiary amine binds H^+ and the N-phenyliminodiacetate moiety complexes Zn^{2+}. The

complexation of each ion results in the retardation of a PET process that otherwise prevents emission from the anthracenyl fluorophore. Crucially, any of these three individual PET process prevents fluoresce. This means that only when all three ions are present above certain levels is a fluorescence emission observed. In logic terms the molecule is a three input AND device driven by Na^+, H^+ and Zn^{2+}. In healthcare terms the delivery of the result by simple irradiation of a fluorescent compound removes the need for expensive equipment, a laboratory technician and a doctor. Whilst the implementation of such a multi-sensing and diagnostic molecule has not been commercially realized yet, the previous section outlined how single-input YES logic gates for H^+, Na^+, K^+ and Ca^{2+} have been deployed worldwide.[103]

Towards multi-valued logic systems

The vast majority of modern computing devices operate based entirely on the binary system – it is commonly used in both hardware and software applications. This limitation – to merely two values (expressed as TRUE and FALSE, on and off or high and low) – may be traced back to a similar dualism found in most of the modern languages. If we take a glance at the very beginning of a scientific history we will realise that works by Aristotle on so called term logic already have established the position of the binary logic.[127] The adopted paradigm allowed for a deterministic description of statements and was both intuitive and simple enough to become a dominant platform for devices and algorithms based on the two-valued Boolean algebra. Nevertheless, even Aristotle, the father of this dyadic approach, was aware of some limitations of his creation.

What we perceive as a great convenience of the binary logic system – the simplicity – is as a matter of fact its main weakness. We understand intuitively that it takes more than two logic values to create a system capable of describing undefined states – this flaw is reflected in the law of excluded middle and in the principle of bivalence.[128] The limitation can be better understood if we take a look at the sea battle paradox – in this problem we eventually reach the point at which a statement cannot be classified as either true or false because it would result in some constraints on free will (we could not influence future events freely). There exists a rather obvious solution to this troublesome situation – we need an additional state representing the uncertainty. It leads us also to the conclusion that the two-valued logic cannot be considered as a universal language; still its domination has been undisputed till the early 20th century.

The most significant attempt to find a better system which would be devoid of described limitations was made by Polish logician Jan Łukasiewicz in 1917.[129] He draw similar conclusions (as presented in the last paragraph) and simply added an unknown state (the solution proposed also by C. S. Peirce).[130] The scientific community followed this concept and a rich background for the multi-valued logic, probability logic, fuzzy logic and other more complex ideas has been created soon after. These new tools proved to be extremely useful as some features of multi-valued systems (both infinite and finite) could be easily associated with fundamental phenomena observed in Nature. Nature provides good examples such as: gene regulation pathways[131] – where the production of proteins is controlled by three different outcomes interpreted as promotion, inhibition and "no effect" – or cell signalling patterns.[132] Another natural implementation of the three-valued logic is the Aymara language used by inhabitants of the Lake Titicaca basin, some parts of Bolivia and Peru. A formal analysis of the Aymara syntax indicates that an additional, third logic value is used in order to express the unknown state[133] – the implementation of the ternary logic distinguish Aymara from the majority of modern languages.

The story behind fuzzy logic is a bit different. After the idea was born and the mathematical formalism capable of dealing with information in a fuzzified form was introduced, it was quickly recognised as a system compatible with the human comprehension. It is actually used naturally in our everyday life, for example when we cannot describe precisely the temperature of an object by using two extremes (cold or hot) and we would rather prefer to choose something in between. Since the fuzzy logic appears to be a good linkage between a strict realm of mathematics and the way we perceive the environment it found numerous applications in devices programmable with the use of linguistic commands which are easily understandable for people (like in the case of thermostats and washing machines).[134]

One important question arises: why we haven't used multi-valued logic systems at the early stages of the computing devices development? From the technological point of view it was simpler and more convenient to apply the binary logic in original electronic circuits[135] – the use of only two states allowed to easily distinguish one from another in a signal pattern spoiled by high noise levels and other distortions. Now, the introduction of new transmission media, especially optical fibres (which allow to encode information by turning the signal off and on and also by changing the light polarization direction), the growing role of optoelectronics and the increased sensitivity of devices (which recognise more subtle features

in the signal), stimulated the discussion on the use of other computational paradigms adopting the multi-valued logic.[136]

Actually, this trend isn't really new as we have witnessed several attempts of the multi-valued logic implementation in the 20th century. A good example is given by studies conducted in the Soviet Union in 1958 when the ternary Setun (Сетунь) was built. In the following years its successors have been introduced (e.g. Сетунь-70), but eventually the programme was abandoned by the order of the USSR authorities.[137, 138] Remarkably, these devices surpassed – if compared in terms of the power consumption and the computing speed – the contemporary binary machines. Not because of its performance, but rather due to some political factors Setun has never been directed to mass production.

These are not the only attempts made to incorporate the ternary logic into both hardware and software designs – the Josephson junction provides us with another interesting example. The circulating superconducting currents can be described not only by their on/off state but also by their direction, thus they may be easily associated with the three-valued system (as it was discussed for the polarised light in optical fibres).[139] The use of such devices could lead to the efficient storage and processing of information based on the balanced ternary system. As for the software implementation, a good example is found among the programming languages, in which the third logic value is introduced (e.g. SQL). This additional state can be expressed as a so called NULL flag which indicates – in SQL databases – that the data is missing, and the result of a comparison with the entry is unknown (it cannot be formally given as true or false).[140]

As it was mentioned before, the use of multi-valued logic systems receives a great deal of attention. Numerous new devices are demonstrated by the scientists, to mention a few: the carbon nanotubes-based pseudo N-Type FETs presented recently by J. Liang et al.,[141] the quantum-dot cellular automaton realizing multi-valued logic operations showed by I. Lebar Bajec, N. Zimic and M. Mraz[142] or encoders constructed with the use of carbon nanotubes FETs proposed by P. Viswa Saidutt et al.[143] At the same time, with all this diversity of different devices, there is a noticeable lack of devices capable of optical signal processing. Actually, the interaction with light, as mentioned before, could immediately reveal the advantages of multi-valued logic systems. In the given example (of optical fibres), the very nature of light favours the ternary logic – it can be polarised in two orthogonal planes and turned off, yielding three logic values. Moreover, if the device is sensitive to irradiation we

may combine an optical input with information encoded in electrical signals obtaining some emergent features. If we additionally use materials which can respond also to the change in chemical environment we could create a system responsive to three independent inputs. A few devices of this kind have been already presented (works by Shutian Liu, Uwe Pischel, Gilles Lemercier)[144, 145][cyt.] but they usually operate in solutions.

Our contribution to the field has been presented just recently – it was the first case of a solid-state system realising two ternary logic gate functions[31] (*accept anything* and *consensus*). The heart of the device was made of a wide band gap semiconductor (*i.e.* titanium dioxide) combined with molecular modifiers. The nanoparticulate film exhibited the photocurrent response that resembled the outputs of two aforementioned logic gates. It was achieved by the purposeful introduction of additional electronic states within the band gap which were associated with cyanocarbon modifiers (hexacyanobutadienide or hexacyano-diazahexadienide anions, denoted as X[.] in Fig. 11) and resulting new excitation path.

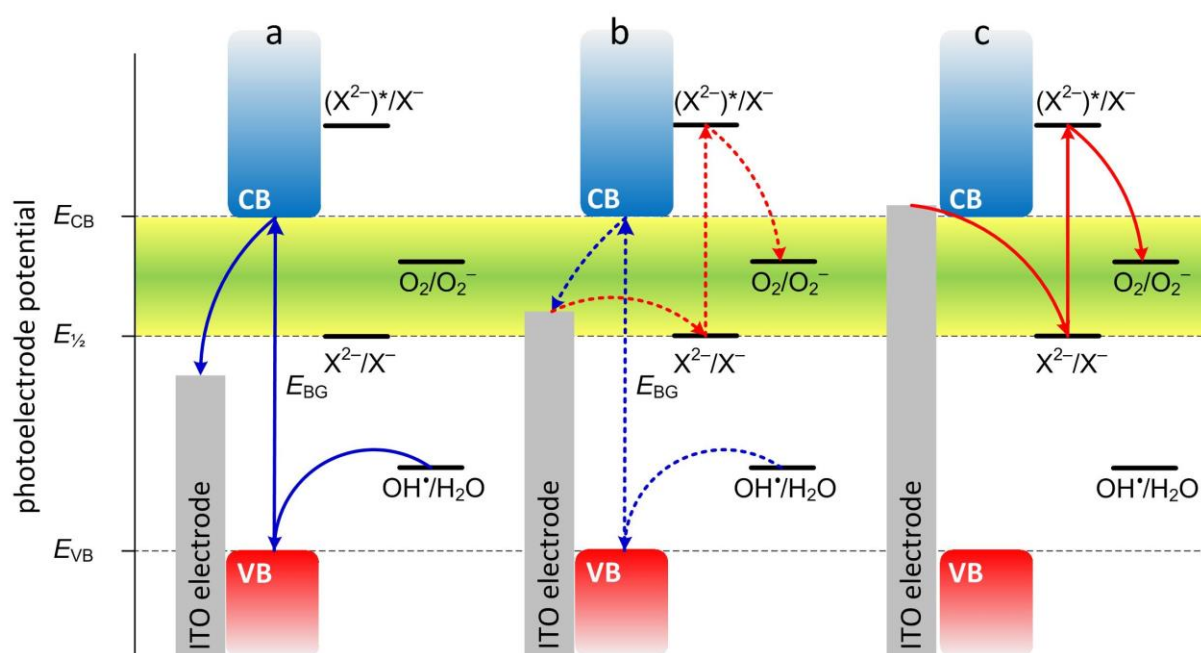*Fig. 13. A simplified energy diagram and the mechanisms responsible for three modes of the photocurrent generation in the system.*

The appearance of an additional excitation path contributing to the photocurrents generation (Fig. 11c) leads to the presence of three distinctive areas in the photocurrent action spectra (Fig. 12). These are of either anodic (Fig. 11a) or cathodic (Fig. 11c) character or the

net photocurrent is close to zero (Fig. 11b). In the last situation the interplay between two competitive processes is responsible for the overall decrease in photocurrents intensity. It may be explained with the use of a model in which two different semiconductors, one of the *n*-type and the second one of the *p*-type, are merged together. If they are active within two different regions of the incident light wavelengths and the electrode potentials, we may obtain a similar result. This unique feature of the system allows us to implement the ternary information processing functions through an appropriate association of the electrical and optical inputs with logic values.

The procedure is similar to the one presented for modified wide band gap semiconductors in the previous paragraphs. Here, we have three values (we will use the balanced ternary logic) – contrary to the binary logic discussed before – which we can assign to three different output ranges recorded for the cyanocarbon modified titanium dioxide electrode. We can label the anodic photocurrents region as logical "1" (TRUE), the cathodic region as logical "-1" (FALSE) and the area with no net photocurrents as logical "0" (UNKNOWN). Such mapping is quite natural as it may be easily related to the mechanisms responsible for the generation of particular signals. The conclusion is supported by the analysis of the situation shown in the Fig. 11b – the competitive character of the processes realized by the *n*-type and the *p*-type parts of the device lead to the unknown state of the system.
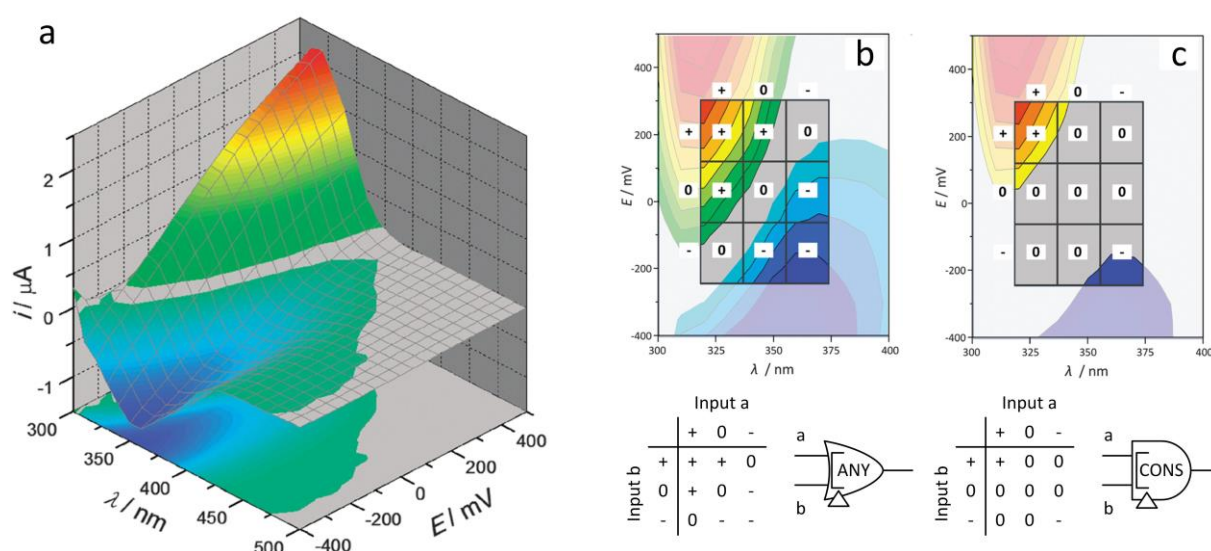

Fig. 14. The photocurrent action map (a) with its interpretation as two dual ternary logic gates: accept anything (b) and consensus (c). The transition between them is done by the change in current intensity threshold. Adapted from Ref. 31.

Both dual gates may be realised within the same system and the transition between them can be done by a simple shift of the current threshold. They may be applied in the design of arithmetic devices, but also – due to a fairly easy concatenation and a possibility to power them through one of the inputs (the energy carried by light pulses) – they may serve as a good starting point for the construction of more complex computing units. Furthermore, the system is immune to undesired feedback loops – by a simple introduction of *e.g.* Schottky diode the unidirectional information flow can be achieved. Similar approach, but based on different hybrid materials enabled the construction of ternary-to-binary decoders and other three-valued logic gates, such as *exclusive OR* gate.

Molecules can also be persuaded to perform ternary logic of a useful kind. For molecular logic-based computation to become established as a research field, it is important to address applications which are barred to semiconductor-based logic devices. One of these incorporates ternary logic, but begins with the simplest binary logic operations.

People within a population are generally identified from their facial features, for twins we might have to look harder or ask a name. Civic matters or travel require certified identification such as a passport. Objects are identified by their characteristics, when we disguise these characteristics or hide them completely by placing them in a box for example, we usually place a label on the box so that it can be easily identified and retrieved. Supermarkets use barcodes to quickly identify goods and reference the price. Computer engineers have gone further taking the identification away from the optical channel and into semiconductor-based paths with Radiofrequency ID chips.[146] These are advantageous as they are machine readable without the need for line of sight. Such tags are commonly used in warehouses for stock control, placed into passports so that biometric data can also be retrieved quickly and easily and are very often found in workplace entry passes. However problems start to arise when the size of the object is reduced. RFID chips are generally useful and cost effective until their dimensions drop below 0.1 mm which leaves smaller objects label-less. We might use an atomic force microscope to engrave smaller objects and an electron micrograph to identify them but it is hard to imagine this as a practical solution.

In order for something to be useful it must be identifiable, in some cases this identification is a spatial address[147] (e.g. wells on a parallel synthesis plate) but in some instances such as combinatorial libraries location identification is not a convenient option. Polymer gel beads are often employed to carry drug or assay candidates during screening and these must be labelled. Cells from patients may also be needed to be identifiable without the

need for gene sequencing. At this level the semiconductor cannot provide a solution – even with further miniaturisation of the component parts, RFID relies on receiving and tranmitting radio frequencies which requires an antenna. To decrease the size of the antenna we must decrease the wavelength of the signal and the shorter the wavelength the smaller the propagation rendering distance reading an impossibility. Thus there is a rather high size limit to the miniaturization of antennas.

The solution to this problem comes first from the world of chemistry. Polymer beads can be tagged with fluorescent dyes allowing us to identify the bead from its excitation/emission spectrum.[148] The problem here is that the molecular excitation/emission spectra are broad and this limits the number of useful colours that can be employed. Using different input/output frequencies allows the handling of larger populations but these are limited very quickly.

A stronger solution is provided by molecular computation.[149] The solution is philosophically simple – ask more than one question during the identification procedure. Each time we shine light (or interrogate an RFID chip) we are asking a question – unfortunately the devices can only answer yes/no and only when the question is phrased correctly. However, beads (or any object) can be tagged with fluorescent PET molecular logic gates and these can respond to more than one question. The questions and answers can be specified as follows:

a) What is the characteristic wavelength of excitation?

370 nm.

b) What is the characteristic output emission wavelength?

420 nm.

c) c) What is the characteristic input (species or property) that interacts productively with the tag?

H^+.

d) What is the Boolean logic type of the input-output profile?

YES.

e) What is the binding strength of the input species as defined by the binding consant?

7.0.

f) What is the pair-wise combination of logic gates (defined by the above questions) which is applied to the object if it is doubly tagged?

PASS 1 + YES.

The answers to questions a) and b) are based solely on the properties of the fluorophore, no significant molecular computation is involved and indeed, this type of system

has been used for tags in combinatorial libraries.[148] The power of the system begins to be exploited when questions are asked of the receptor component, about its acid sensitivity and if so at what pH does the switching occur? Does the tag require an ion? If so what ion? What concentration of ion does it require? Does it require more than one input? Does the input switch fluorescence 'on' or 'off'? All of these questions are being addressed to a single molecular tag and the tag is responding with one of two answers 'yes' or 'no', fluorescence 'on' or 'off", '1' or '0'.

This system has been demonstrated with Tentagel[TM] beads 0.1 mm diameter tagged with H^+-driven YES, PASS 1 and NOT logic gates (**11**, **12** and **13** respectively) (Fig. 15).[149] The PASS 1 gate is devoid of a receptor and fluoresces regardless of the pH while for the YES gate a PET process from the amine to the fluorophore is blocked by protonation. The NOT gate works in reverse fashion - protonation of the pyridyl unit launches a PET process from the fluorophore quenching fluorescence.
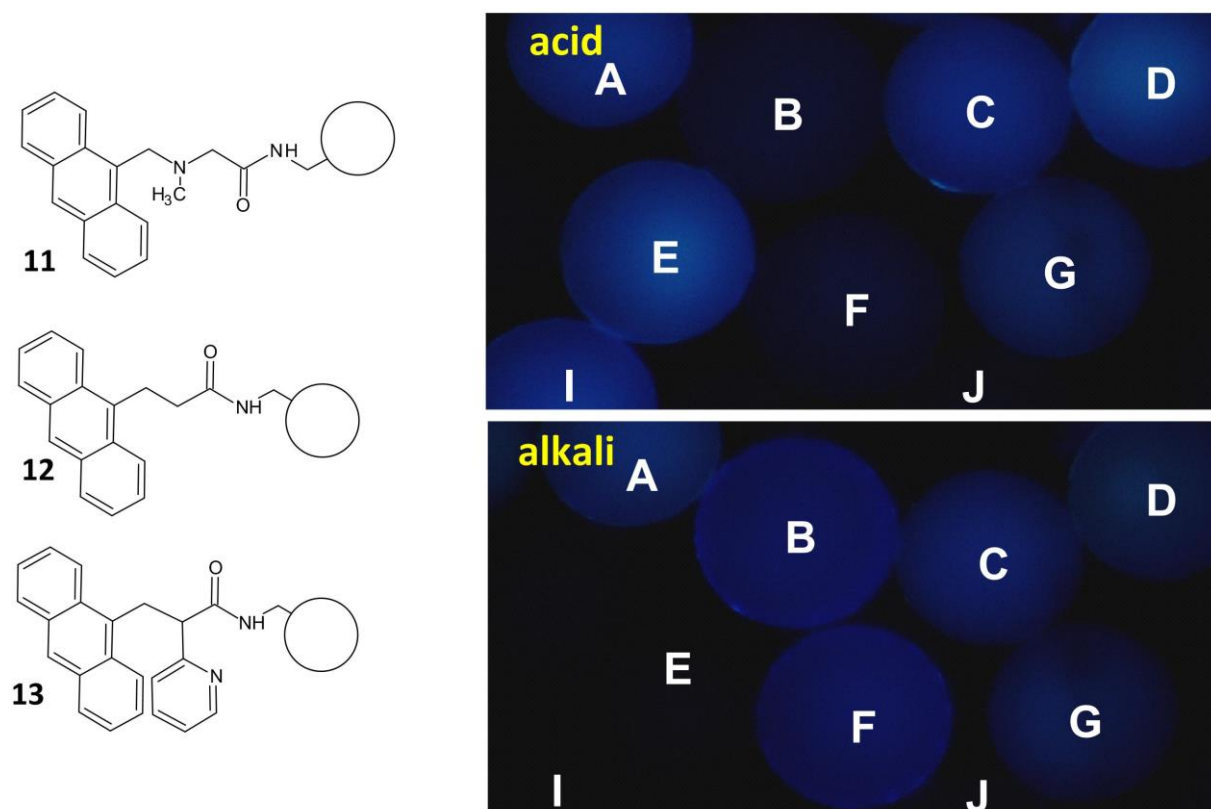

*Fig. 15. The molecular structures of MCID tags **11-13**[149] and their use in distinguishing tagged beads with pH-dependent fluorescence microscopy. The logic type of each bead is A; PASS 1, B; NOT, C; PASS 1, D; PASS 1 + YES (1:1), E; YES, F; NOT, G; PASS 1, I; YES, J; PASS 0. Photograph adapted from ref. 149.*

In this monochromatic system the beads tagged with **11**, **12** and **13** are clearly distinguishable through a few simple tests. Variation of the tag allows large numbers of objects to be quickly and easily identified in this way. The combination of input/output frequencies, types of logic, input chemicals and threshold values gives rise to thousands of distinguishable tags - a number that cannot be approached with colour alone. It is however, only with the realization that beads may be tagged with more than one tag (or with different ratios of the same pair of tags) that the true power of the system becomes evident. The output of these systems relies on a single measurement of fluorescence intensity and this single measurement means that multi-valued logic derived from summed output can be used.[150]

In modern computing the serial integration of vast numbers of logic gates means that accummulated errors during reading prevent the use of such higher-valued logic. Every measurement has an associated error, and when one measurement is the basis for the next these errors mount quickly. The result of such elongated serial measurement is that only the presence or absence of a phenomenon can be distinguished. Thus the practical world of electronics is binary. Since this system needs only to make a few simple measurements of emission intensity (each with an error of ca 1%) and the number of sequential measurements is low the overall error remains below 10%. As any two logic gates can be easily arrayed into five easily distinguishable tags based upon the ratio of each (1:1, 1:2, 2:1, 1:0 and 0:1) we can potentially generate millions of unique tags, which can be identified through five experimental quantities (excitation wavelength).(emission wavelength).(logic type and combination).(inputs).(binding threshold for each input).

The first steps into fuzzy logic…

As stated before, information processing structures designed by Nature operate based not only on the two-valued logic but also incorporate some more complex systems. It is fairly easy to find numerous examples of such biological devices in our surroundings, but also in our bodies – the perception of external signals bases on the chunks of information which are very often imprecise. The sensors and receptors responsible for the communication with the environment provide our central nervous system with data which may be noisy or even incomplete – mainly due to some fundamental limitations of our bodies (*e.g.* the limited concentration of sensors per area unit, the signal attenuation during the transmission, *etc.*). Despite this, our brain is capable of interpreting these inputs and creating a complete and meaningful picture of the situation.[151] As a matter of fact, the brain is so efficient that we are

able to process information at the level surpassing the performance of the most powerful computers (it refers to cognitive functions considered in a broader sense, as we can no longer compete with modern supercomputers in terms of the raw computational power).[152]

It was mentioned in the previous paragraph, that some features of the binary system – such as the rule of excluded middle[128] – entail certain limitations which make the proper description of real situations impossible. Ultimately, that may lead to paradoxes or false dichotomies. An instant remedy for this problem may be provided by the multi-valued logic, but it does not eliminate all the obstacles – even in the case of a greater number of logic states, we are still entitled to play only with crisp and well-defined values. The description of the real world demands something more general – the system in which some level of vagueness exist and the truth depends on the reasoning process (as in the case of sensory systems of various people – the same set of input signals may be interpreted in a different way). It leads us to the conclusion that a paradigm which allows us to assign particular elements to different sets is required.

Similar reasoning led to the introduction of the fuzzy logic by Zadeh in 1965[153] – it is noteworthy that several other mathematicians (such as Tarski, Łukasiewicz or Russell) have studied some elements of the fuzzy logic before.[129, 154] The most important feature of the system is its ability to convert the quantitative data into the qualitative, descriptive forms which may be interpreted in terms of human-like linguistic rules. That induced a development of a strict mathematical formalism encapsulating very natural (from the human perspective) logic. The concept was further expanded by Mamdani in 1975[155] and with several minor modifications has been used since then. It is particularly useful in systems which operation principle bases on the interaction with a user and it is implemented in numerous control algorithms and in some artificial intelligence systems.[156]

As the interest in the fuzzy logic increased the system has been applied in various hardware and software implementations. In an addition to engineering solutions it has been considered as a good candidate for simulations and modelling of some fundamental phenomena found in biological structures. A promising extension to this idea is provided by the chosen concepts taken from the field of molecular electronics – when combined with the fuzzy logic approach it can serve as a platform facilitating the research on functions of biological neural networks and sensory systems.

The efforts to merge molecular electronics with the fuzzy logic systems (FLS) have been made by researchers like Gentili[151, 152, 157-162] and Deaton[163] at the beginning of the century and just recently by Zadegan[164]. A next step in the process, which seems natural, is adapting FLS on the ground of solid-state devices based on hybrid materials made of metallic/semiconducting nanostructures combined with molecular modifiers. Here, the PEPS effect may prove useful.
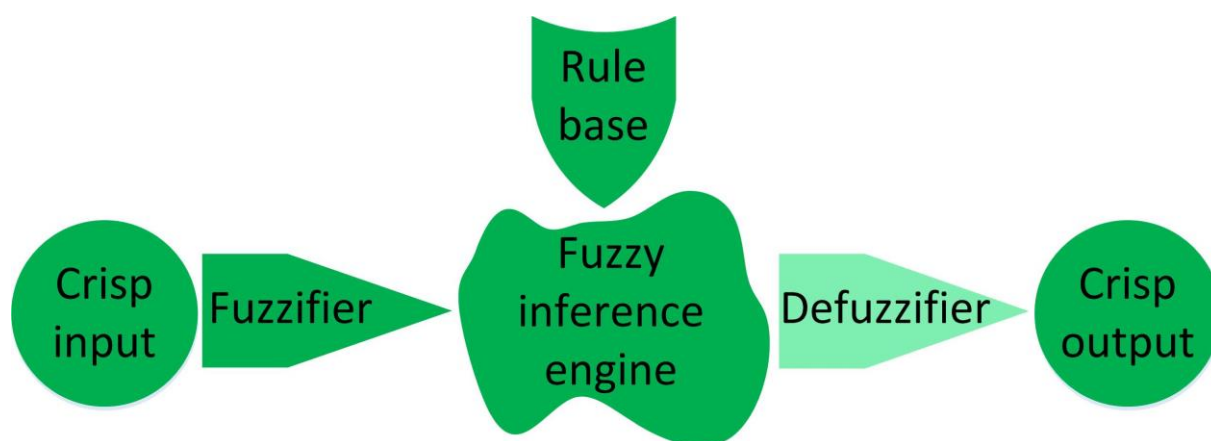

Fig. 16. The schematic representation of a fuzzy logic system. The presence of the defuzzifier is optional and it can be removed from the FLS if Takagi-Sugeno inference is applied or if the expert system is expected to provide a linguistic output.

Both, inputs and outputs of ordinary systems exhibiting the PEPS effect may be expressed by functions which are smooth (they are continuous and differentiable). It makes it possible to divide the variables ranges into regions, which may be labelled in the process of fuzzification. Thanks to the linguistic rules provided by a rules base we may operate on these newly created sets (and labels) inside a fuzzy inference machine. Finally, according to the purpose and the elements of the FLS, we may obtain a crisp output (in the case of Takagi-Sugeno approach), we may decide to defuzzify the results (in the case of Mamdami system), or to leave the output in a linguistic form (Fig. 16).

In the step called fuzzification we assign membership functions to the crisp values and label them (Fig. 17). The process is similar to the one presented by Gentili[157] for fuzzy logic systems realised with the use of intermolecular interactions. Here we used FuzzyLite library with QTFuzzyLite graphic user interface and XFuzzy 3.3 design tool. We apply triangular and

trapezoidal type membership functions and formulate normal, convex fuzzy sets – the resulting partition is presented in Fig. 17.
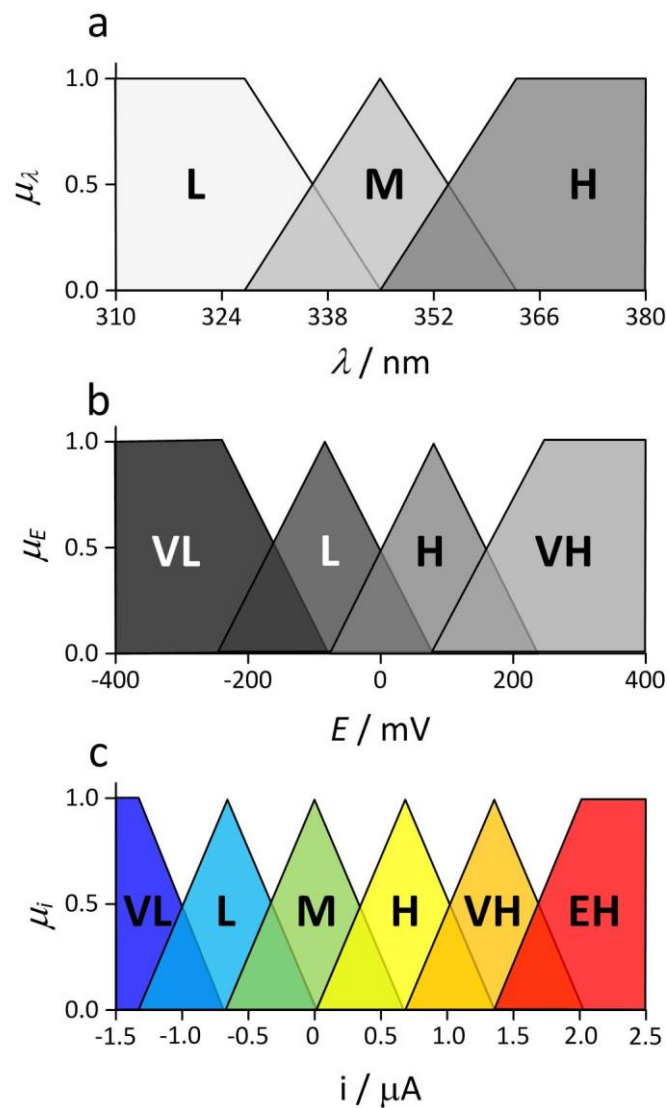
Fig. 17. The result of the variables division in fuzzy sets for both inputs – (a) the wavelength of incident light and (b) the electrode potential – and (c) the generated photocurrent. The ordinates show the membership functions values and the labels are correlated with the symbols used in Table 4 – Very Low (VL), Low (L), Medium (M), High (H), Very High (VH) and Extremely High (EH).

Noteworthy, the partitions for the system output (Fig. 17c) recreate the photocurrent map presented in Fig. 14 with signal intensities assigned to six presented ranges labelled as *Very Low (VL), Low (L), Medium (M), High (H), Very High (VH) and Extremely High (EH).*

To create the Mamdani-type FLS we need to formulate the linguistic rules, which are used to map the input onto the output inside the inference engine. These rules can be expressed as IF…THEN… statements in which the first part is called the antecedent (or the premise) and the second one is called the consequence (or the conclusion). In order to connect multiple antecedents we may use three basic operators – AND, OR and NOT. In the case of more complex rules bases and/or an expanded data set, we can introduce weights that role is to strengthen or weaken certain implications. This procedure prevents us from the situation in which the premise will lead to different conclusions, thus the statements would lead to contradictions. Our system is fairly simple, hence this step may be omitted.

One of the most important phases in the design of the FLS is a formulation of rules – these may be expressed in various ways for the situation depicted in Fig. 17. For simplicity, it is a good policy to split complex implications into simplified forms. An example is showed below – the instruction (4a) can be converted into three more elementary statements linked only with the AND operator (4b). From the mathematical point of view, this interchangeability is nontrivial, as it depends on the selected definitions of t-norm and s-norm. At the same time, we probably recognise this equivalence – from the linguistic viewpoint – as quite obvious.

IF (λ=H **AND** E=VL) **OR** (λ=M **AND** E=VL) **OR** (λ=H **AND** E=L) **THEN** i=VL   (4a)

IF λ=H **AND** E=VL **THEN** i=VL

IF λ=M **AND** E=VL **THEN** i=VL   (4b)

IF λ=H **AND** E=L **THEN** i=VL

The clarity of such representation of the rules base is paid for with its complexity in the case of a larger number of labels. An alternative form can be adapted when we decide on only one operator connecting the inputs – the rules base may be represent in such structure by the matrix. In the presented situation we may try to simplify the system by choosing only the AND operator and creating a rules base matrix as presented in Table 4. As there are two independent inputs with three and four labels (for wavelengths and potentials respectively) we will obtain 3×4 matrix as the result.

Table 4. The rules base matrix for the fuzzy logic system based on the photocurrents map presented in Fig. 14.

		potential			
		VL	**L**	**H**	**VH**
wavelength	**L**	L	H	VH	EH
	M	VL	L	M	M
	H	VL	VL	L	M

With the rules base prepared and the fuzzy sets we can make calculations on, we only need to start our inference engine to get the results in a linguistic form. As mentioned before, we may want to translate the output back into crisp values. To do so we need to add a defuzzification block to our scheme. That presents an additional degree of freedom in the FLS as we may choose from a great variety of methods. If we select appropriately, the FLS may be used as so called approximator which will give expected intensities of the generated photocurrent when fed with input values in a fuzzified form. We may even try to recreate the photocurrent map presented in Fig. 14. The result of such procedure is shown in Fig. 18. We can notice some resemblance between both graphs, as the main features of the experimental data are fully reproduced.
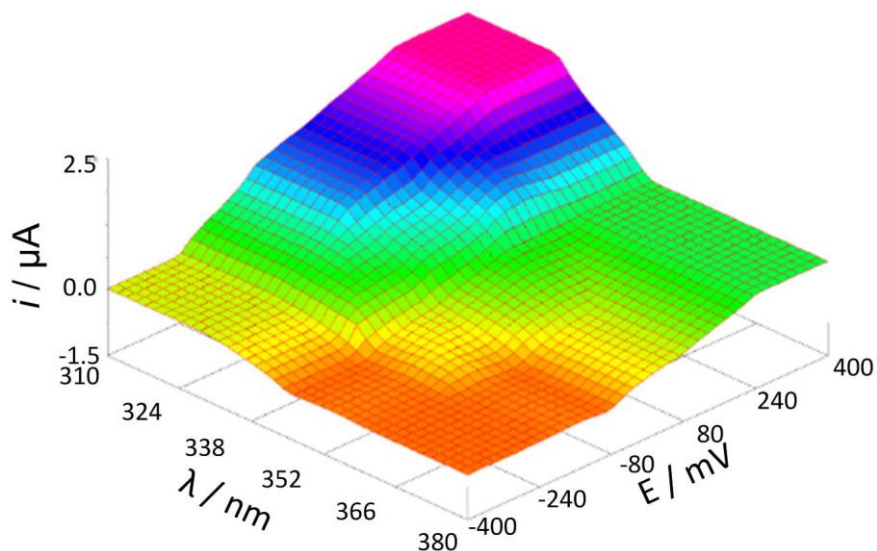

Fig. 18. The output of the fuzzy inference system used as an approximator for the reproduction of the experimental results shown in Fig. 14.

The discussed fuzzy logic system is fairly uncomplicated – it consists of relatively small fuzzy sets with only a few membership functions (labels) and the simple rules base. T-norm and s-norm operations are defined here in a standard way (*i.e.* the minimum for conjunction and the maximum for disjunction), we chose basic accumulation and implication approaches (the maximum and the minimum respectively) and used the defuzzification procedure based on the centroid method. Even with these simplifications we are able to reproduce some of the most important features of the experimental data. Obviously, the FLS may be further optimised to enhance its prediction capabilities by an appropriate tuning of the aforementioned parameters.

It is also possible to change the FLS behaviour by the addition of some other features – one of the useful examples are hedges.[165] These additional terms are introduced inside the rules base and have an impact on the membership function shape. They may be expressed in the form of adverbs such as: very, slightly, somewhat, etc. To further enhance the information processing capabilities of the FLS we may combine it with some concepts taken from neural networks which results in so called neural adaptive fuzzy inference systems. These are capable of membership functions optimisation based on the learning procedures adopted.[166, 167]

…and other human-level computing

The ultimate goal for researches working on information processing systems it to mimic the functions of biological neural networks and other human-level cognitive functionalities. As mentioned in the previous paragraphs, the modern supercomputers surpassed our capabilities in terms of the raw computational speed and efficiency (by the order of magnitude).[168] Nevertheless, some features of our perception and cognitive functions make our brain more versatile than the fastest machines. The central nervous system is prepared to deal with big chunks of information of various nature, often with some level of incompleteness, and synthesise it into a meaningful output (a good example is the pattern recognition performed by the brain).

The major advantage – if the learning efficiency is considered – of biological structures over artificial devices results from their plasticity.[169-172] It is, in simple words, caused by the capability to create new information transfer pathways (through synaptic

connections) which facilitates reasoning processes. This superiority can be also explained by the differences in used computation paradigms – our nervous system is versatile in this matter and does not limit itself to only binary bits (*e.g.* the sensory system deals with some level of uncertainty and information fuzzification). At this moment, that kind of plasticity is a unique feature of biological structures and has not been mimicked successfully in any artificial system yet.[172]

A lot of effort has been put to create algorithms with similar functionalities and some of these attempts have been successful. The neural networks (NN) are the best example of such system, as they can be used (after an appropriate training) as approximators, pattern and sequence recognition systems, etc. The NNs have been applied in various control software implementations at the technological and production level and in prototypic devices such as an artificial nose (used for sensing chemicals found in drugs, explosives, etc.). The NNs provided also a good starting point for more complex ideas, such as the hierarchical temporal memory (HTM), which is basically a combination of certain concepts from the NNs and some biomimetic features (*e.g.* the architecture of the neocortex) and offers a new quality, which already has proved to be extremely useful.[173, 174]

The HTM networks are essentially the multi-level matrices composed of simple computing units which are stacked in a hierarchical manner to provide an advanced information processing resembling the functions of the cerebral cortex. In this biological structure information is translated between several circuits (typically we distinguish six main layers) and undergo bottom-up, top-down and horizontal interactions. This approach allows a single node to be numerically inefficient and is based mainly on the collective, synergetic behaviour of the network as a whole. The concept may be associated with the idea of a 'smart dust' introduced by Kristofer Pister in 1997.[175] It bases on the use of a large number of relatively small (~1 mm^3), ubiquitous and autonomous computing devices, which are provided with a sensory system, processing units, memory and communication capabilities. Together, they create a dynamic mobile network. The idea was retransformed and further developed when new sensing and labelling nanostructures have become available.[176, 177] Eventually, the 'smart dust' has reached a substantial level of complexity when nanoparticles have been merged with functional biomolecules.[178-182] Similar hybrids have been used not only as sensors but also as simple logic devices made of micellar and liposomic structures combined with molecular sensors, switches and logic gates.[183-185]

On the other hand, some features of human reasoning may be described on the ground of the fuzzy logic – as already explained the brain works on data which is often incomplete and interfered by noise and its interpretation is realised based on implications written in something we can call a rules base. If we take one step back in terms of complexity, we will notice that the information processing performed at the synaptic level can also be described by this paradigm. It has led some researchers to the conclusion that it should be possible to model some of the features of biological neural networks within chemical systems which behaviour would be interpreted in terms of the fuzzy logic.[151] This applies also to bio- and chemosensors built with the use of molecular structures and nanoparticles which could be used as models for the sensory systems found in nature.

The problem may be also approached form another direction when we focus more on the structure of connections within biological neural networks rather than algorithms governing the communication. It may be realised with several hybrid materials combined together with different interfaces between them, which would mimic complex systems found in living organisms. These unitary cells can be provided with processing units and memory cells/memristive elements. Such prototypic devices have been already created, nonetheless in most of the cases information is processed in the form of chemical and electrical signals and no light sensitivity is implemented. These devices are also significantly slower than the individual building blocks of biological structures.[186-192]

A good platform, which would allow the design of optoelectronic devices exhibiting the behaviour similar to synaptic structures, could be provided by systems utilizing the PEPS effect. These may be programmed with light, thus extending the range of possible interactions by optical stimuli. They have also other advantages – as it was explained in previous paragraphs these photoactive cells may be fairly easy concatenated into more complex networks and the energy needed for the operation can be provided through one of their inputs. That makes the reconstruction of even extensive neural networks a reasonably simple task. The experimental results obtained for numerous hybrid materials exhibiting the PEPS effect and time-dependant photocurrent generation profiles show that these nanocomposites may be used to mimic synapse-like behaviour in fully artificial systems which are also light sensitive.

One of the hybrids exhibiting the PEPS effect is the system made of cadmium sulphide nanoparticles modified with thermally activated multi-walled carbon nanotubes combined with an appropriate ionic liquid. This nanocomposite fused into a sandwich-like device

displays a Hebbian-like plasticity[193] which is characteristic for natural synapses. The experimental results indicate that this unique feature results from a subtle equilibrium between charge trapping/detrapping processes and mechanisms controlled by the diffusion. We verified this assumption in a numerical experiment, in which the equivalent circuit was examined and the response to the pulsed stimuli was calculated.

The experiment involved optical stimulation of the sample with short (approx. 100 µs) pulses of blue light. The sandwich-like device was made of CdS/MWCNT hybrid[14, 194] deposited onto ITO@PET foil and covered with another slide of ITO@PET with the semi-solid electrolyte (Fig. 19). Under irradiation, the system generated anodic photocurrent spikes, which profile strongly depended on the input time characteristics (*i.e.* number of pulses, their length and the interval between them).
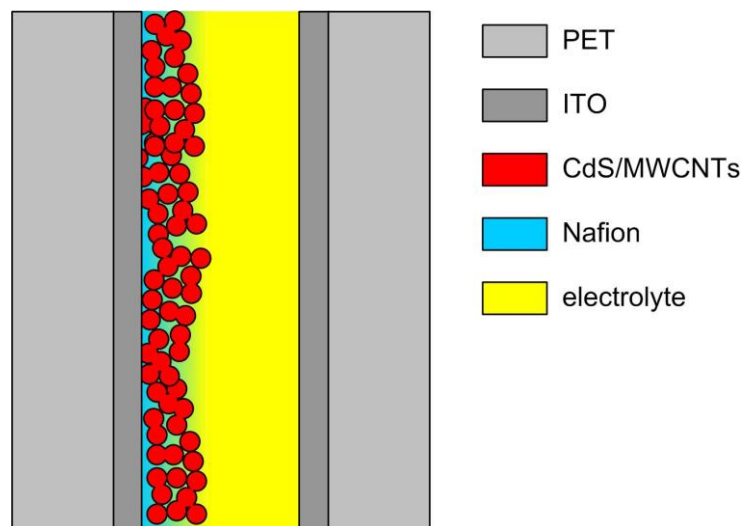

Fig. 19. The schematic representation of a photoactive sandwich-like device exhibiting synapse-like behaviour.

The changes in a photocurrent profile resemble the response of certain types of synapses – it relays on the time correlation between incident spikes. Furthermore, we may observe two types of plasticity – as described by the spike-timing-dependant plasticity (STDP) rule[195] – with an enhancement of the consecutive photocurrent spikes intensity (the potentiation) or with the decreasing intensity of the subsequent signals (the depression). The behaviour depends mainly on the electrical state of the device – the electrode potential – but also on the timing of the optical stimulus (Fig. 20). That feature is very similar to the operation modes found in the biological synapses.
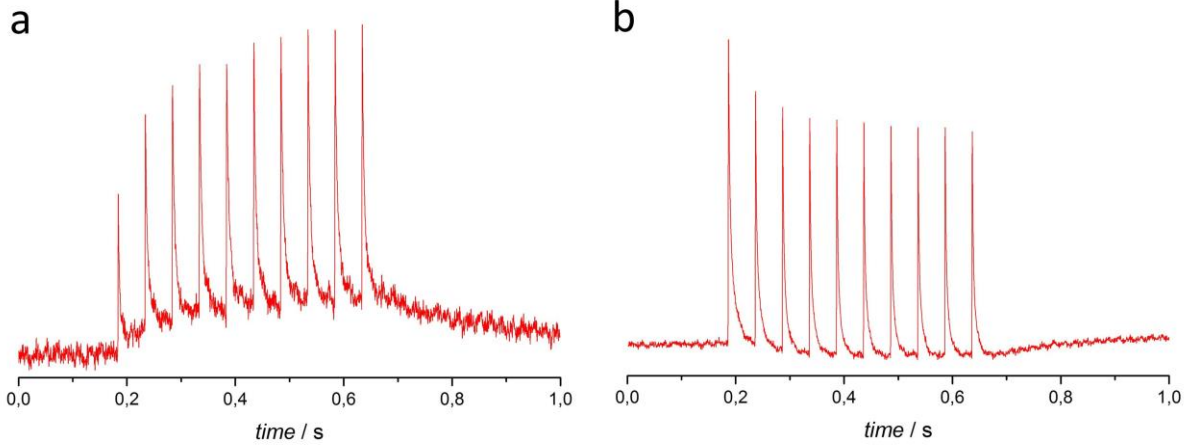
Fig. 20. Two modes of plasticity – (a) the potentiation and (b) the depression – realised with the use of a fully artificial system composed of CdS/MWCNT hybrid and ionic liquid. The switching between both situations occurs when the applied potential is changed.

If we consider the information processing performed by biological structures, we may simulate the output profile, provided that we will assume the type of a synapse and we will approximate its internal parameters. Particularly, we may access the information on the relative intensities of consecutive spikes in series – that is we factor we will use to investigate our systems response. In a basic version of the equation coupling amplitudes of neighbouring signals (called the learning window) provided by the STDP model the I_2/I_1 ratio can be described by the combination of exponential functions.[196] The experimental data were analysed based on the equation presented below, expressing the increase/decrease of the second spike intensity compared to the first one in series (equation 5):

$$f(\Delta t) = \alpha_1 \exp\left(-\frac{\Delta t}{T_1}\right) + \alpha_2 \exp\left(-\frac{\Delta t}{T_2}\right) + \beta \tag{5}$$

where Δt is the time interval between the first two spikes in series, $\alpha_{1,2}$ are the parameters related to synaptic weights and $T_{1,2}$ may be interpreted as the characteristic time constants. The fitting procedure yielded parameters: $\alpha_1 = 3.014 \pm 0.034$, $\alpha_2 = 4.80 \pm 0.21$, $T_1 = 116.4 \pm 3.7$ ms, $T_2 = 6.88 \pm 0.31$ ms and $\beta = 1.722 \pm 0.024$. It is remarkable that the time constants coincide with the values found in biological structures. The result shows that the presented device mimics the behaviour characteristic for natural synapses.[197]

The postulated mechanism responsible for the observed behaviour (based on the charge trapping/detrapping processes) was verified with the use of a numerical experiment in which the equivalent circuit was proposed (Fig. 21a). It consist of three RC loops, two resistors playing a role of the ohmic resistance of electrolyte and CdS/MWCNT junctions and two diodes resembling the Schottky junctions between the support and the hybrid material and between MCNTs and CdS nanoparticles.[20, 23, 198] Upon pulsed stimulation of the circuit, the experimental result was recreated including the potentiation of current spikes with a decrease in the interval between consecutive signals (Fig. 21b and 21c). We also managed to explain the role of trapping states in the systems, as the removal of the branch responsible for these events (marked with a red line in Fig. 21a) results in a drastic change of the output. It appears that these processes are crucial for the synaptic plasticity – without the red branch the recorded response is similar to the signal given out by the unmodified semiconductor with no signs of any memory effects.
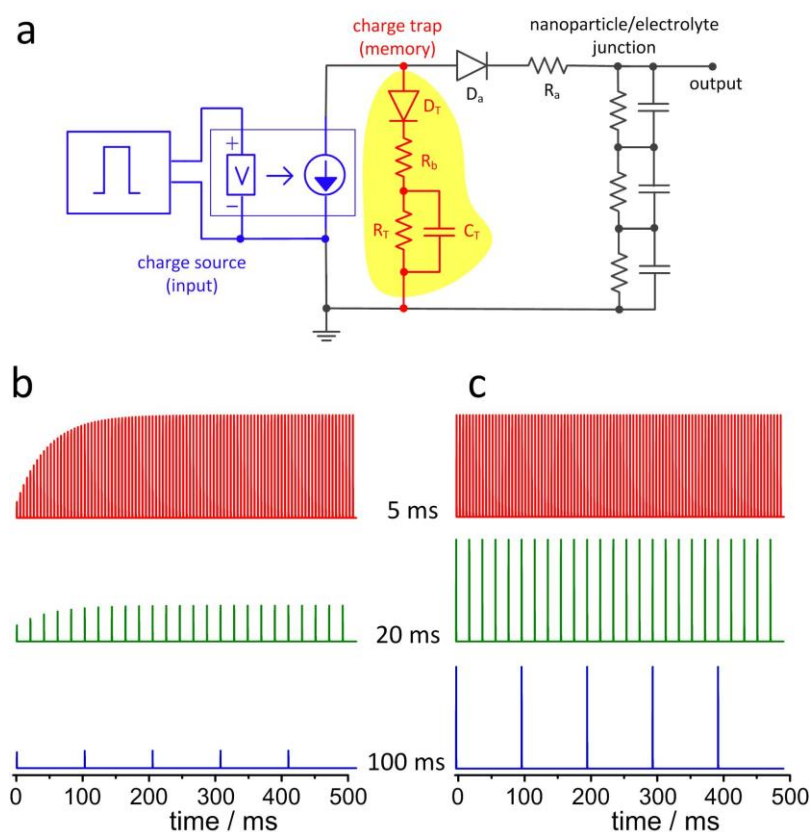

Fig. 21. The equivalent circuit for ITO/MWCNTs/CdS hybrid electrode used in the numerical experiment (a). The results of the simulation done for the system with (b) and without (c) a branch responsible for trapping/detrapping events (highlighted fragment of the circuit).

With this new insight into the nature of interactions within the examined system we postulated an energetic diagram which describes the interplay between individual processes. First of all, the profile of an individual photocurrent spike is unaffected by the changes in the stimulus parameters. We also know that the photocurrent action spectrum is insensitive to the addition of multi-walled carbon nanotubes to the cadmium sulphide. It leads to a conclusion that the CdS nanoparticles are entirely responsible for the generation of photocurrents and MWCNTs play a role of charge trapping/detrapping agents. The photoelectrochemical cycle is closed by the redox-active species present in electrolyte which also control the time resolution of the memory effect throughout the diffusion process (Fig. 22).
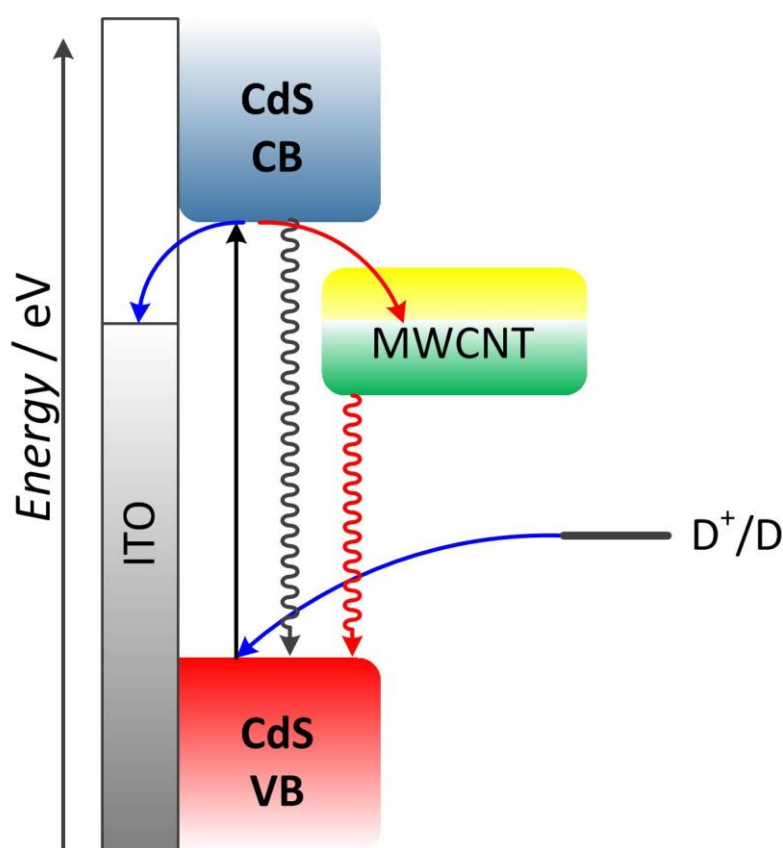
Fig. 22. The energetic diagram with the postulated mechanism responsible for the observed synapse-like behaviour.

The devices may be easily concatenated to form systems of a greater complexity. These are supposed to realise more sophisticated functions as the interactions between individual nodes should result in the information processing interference and some sort of the self-programming. In the next step, we would expect the enhancement of the learning

capabilities of such superstructures. That kind of matrices will be built in a near future from semiconductors active in different wavelength ranges and various molecular modifiers. This will allow the use of numerous optical inputs coupled together and – hopefully – we will observe some emergent features of the system.

Simple molecular systems have also been recently persuaded to carry out several human-level computations. For instance, edge detection is a nearly continuous process in our own visual perception, even though it occurs at a subconscious level. It is carried out in the retina of our eyes within milliseconds allowing us to quickly evaluate objects for their threat potential.[199, 200] The retina contains layered cells with rod and cone cells on the surface which an image is received and then passed to ganglion cells, which in turn send the image down the optic nerve to the brain. Within the millisecond timeframe, a wiring system is called into action where a group of rod and cone cells pass their signals on to a single ganglion cell. This output is only sent to the optic nerve if the central rod or cone cell is illuminated while surrounding cells are in the dark (or vice versa). The edges, which are extracted in this manner and sent to the brain, contain far less information than the full image. This makes it easier for the brain to quickly identify the edge pattern by comparing it to other edge patterns held in easily accessible memory.[201] Once identified the appropriate activation of muscles can enable the appropriate response, e.g. to run away.

Edge detection can be mimicked in a semiconductor computing context but it requires a full stored-program computer[104, 105] with edge detection software such as the Canny algorithm.[202] It is worth emphasizing that a logic gate array alone will not do. It has also been emulated by films of genetically modified bacteria[203] and also by reactive networks of high molecular-mass oligonucleotides.[204] Both of these examples require high levels of organisation in space-time which are characteristic of living systems. The edge detection emulation achieved with small molecules involved their simple spreading on filter paper.[205] The molecular system used consisted of a photoacid generator (triphenylsulfonium chloride[206]) and a H^+-driven 'off-on' fluorescent sensor.[207, 208] A weak pH buffer (a dilute solution of Na_2CO_3) was used to hold the sensor in an 'off' fluorescent state before an object is projected onto the paper with 254 nm light. It is critically important that the filter paper is soaked in the solution of the mixture of compounds in methanol:water (1:1, v/v) and then dried for 4 minutes at 50 C. The projection with 254 nm light allows an image of the object to be written on the paper. After writing for a certain amount of time, a fluorescent outline of that object is seen when read under 366 nm illumination. It is notable that a common two-

colour ultraviolet lamp is used to project the object during writing and to read the information presented, so that the experiment is extremely convenient and inexpensive to carry out.

Writing with 254 nm causes the photoacid generator to produce H^+ in the irradiated area. The weak buffer is eventually overcome by the increasing H^+ concentration which then switches the fluorescent sensor 'on' from its initial 'off' state. The switching 'on' occurs when the PET process from the amine side groups to the perylenetetracarboxydiimide lumophore within **14**[207, 208] is stopped. This produces a positive photograph of the projected object for short irradiation times. Further irradiation causes a build-up of another product of the photoacid generator. It is electron rich allowing it to take part in a bimolecular PET process thus quenching the fluorescence of protonated **14** and switching it 'off' again. A fluorescent edge is produced as some protons diffuse across from the irradiated area to the non-irradiated area down their concentration gradient. This can be thought of as an acid front slowly spreading outwards while neutralizing the local pH buffer and leaving behind the heavier quencher product, which causes switching 'on' of fluorescence on the non-irradiated side of the edges to a distance of 1-2 mm only.
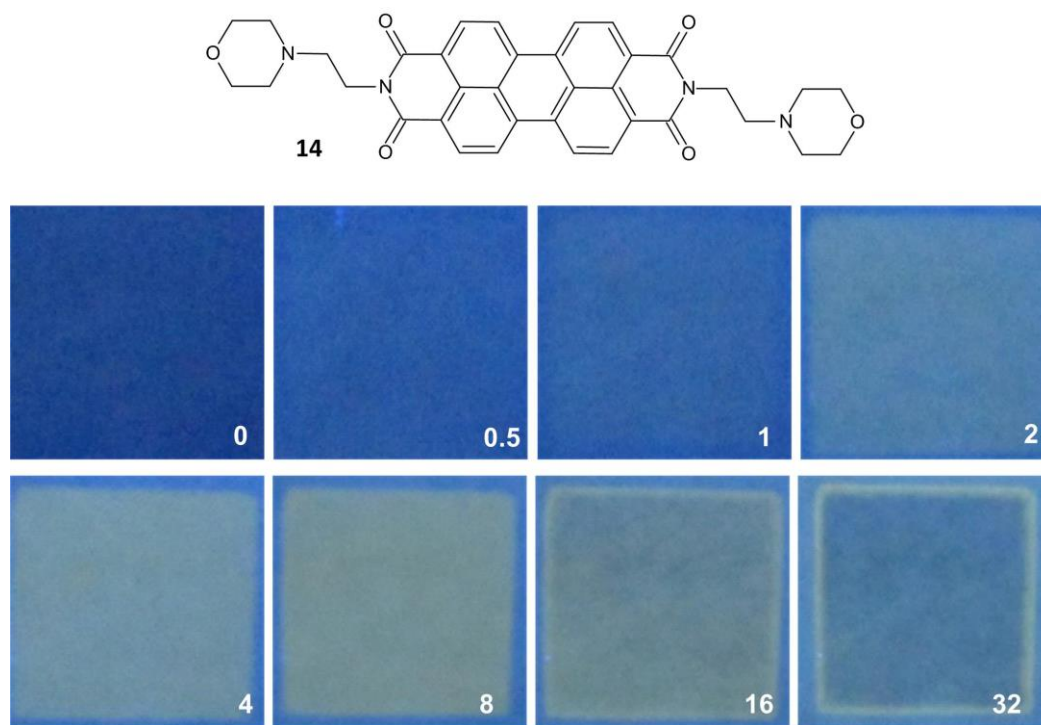

*Fig. 23. The molecular structure of **14**[205] and the photographic result of writing a 'square' object onto a paper containing **14**, triphenylsulfonium chloride and Na₂CO₃ for the stated times, followed by reading under 366 nm light. Scale bar = 4.0 cm. Photograph adapted from ref. 205.*

The processes outlined in the previous paragraphs can be put on a rather quantitative footing by detailed modelling based on simple foundations. pH profiles of acid-base titration, pH-dependent fluorescence of 'off-on' sensors, Stern-Volmer-type bimolecular quenching as well as Fick-type diffusion form the four pillars of these foundations.[208]

The fluorescence in the irradiated regions can be decribed as an 'off-on-off' process driven by the writing light dose. 'Off-on-off' processes are common[209-214] and can be understood as XOR logic behaviour.[2, 3] They are common and can be seen in enzyme activity as a function of pH or in tunnel diode currents as a function of voltage.[214] However, the fluorescence in the edge region itself is logically much more complex and is best described in terms of the Canny algorithm running on a full computer so that various subroutines can be called out at different stages of the run to be executed on different logic gate arrays within the central processing unit. The role that the filter paper plays as a graphic user interface during this image processing application also must not be forgotten. Just like 'off-on-off' processes 'off-medium-high' variants[215,216] are likely to be exploitable in similar contexts.

Subconscious human processes such as edge detection appear to be closely bound up in conscious human activities such as outline drawing. Virtually all children who have been on earth have drawn outlines with a finger on sand or with a crayon on paper. A few of them have grown up to be a Michaelangelo or a Leonardo who give pleasure to many millions. Even many of their masterpieces started life as a simple cartoon or sketch which is essentially an outline drawing. Our molecular edge detection system involving **14** is therefore easily put to work to perform this outline drawing task.[208] Line drawings with rather intricate curves and angles are faithfully achieved. We can happily conclude that the ability to get small simple molecules to carry out complicated human-level computations is an intiguing prospect and provides scope to achieve other similar processes in the future.

Acknowledgements

References

1. G. Boole, *An investigation of the laws of thought of which are founded the mathematical theories of logic and probabilities*, Walton and Maberley, London, 1854.
2. K. Szaciłowski, *Infochemistry. Information Processing at the Nanoscale*, John Wiley & Sons, Chichester, 2012.
3. A. P. de Silva, *Molecular logic-based computation*, Royal Chemical Society, Cambridge, 2013.
4. S. Somasundaram, C. R. Chenthamarakshan, N. R. de Tacconi, Y. Ming and K. Rajeshwar, *Chem. Mater.*, 2004, **16**, 3846-3852.
5. N. R. de Tacconi, C. R. Chenthamarakshan, K. Rajeshwar and E. J. Tacconi, *J. Phys. Chem. B*, 2005, **109**, 11953-11960.
6. K. Rajeshwar, N. R. de Tacconi and C. R. Chenthamarakshan, *Curr. Opin. Solid State*, 2004, **8**, 173-182.
7. S. K. Poznyak and A. I. Kulak, *Electrochim. Acta*, 1990, **35**, 1941-1947.
8. K. Szaciłowski and W. Macyk, *Comp. Rend. Chimie*, 2006, **9**, 315-324.
9. P. Kwolek, K. Pilarczyk, T. Tokarski, K. Lewandowska and K. Szacilowski, *Nanoscale*, 2014, **6**, 2244-2254.
10. P. Kwolek, K. Pilarczyk, T. Tokarski, M. Lapczynska, M. Pacia and K. Szacilowski, *J. Mater. Chem. C*, 2015, **3**, 2614-2623.
11. P. Kwolek and K. Szaciłowski, *Electrochim. Acta*, 2013, **104**, 448-453.
12. B. Lu and Y. Zhu, *Phys. Chem. Chem. Phys*, 2014, **16**, 16509-16514.
13. P. Kwolek, K. Pilarczyk, T. Tokarski, J. Mech, J. Irzmański and K. Szaciłowsk, *Nanotechnology*, 2015, **26**, 105710-105719.
14. A. Podborska, B. Gaweł, Ł. Pietrzak, I. B. Szymańska, J. K. Jeszka, W. Łasocha and K. Szaciłowski, *J. Phys. Chem. C*, 2009, **113**, 6774-6784.
15. M. El Harakeh, L. Alawieh, S. Saouma and L. I. Halaoui, *Phys. Chem. Chem. Phys*, 2009, **11**, 5962-5973.
16. S. Ogawa, K. Hu, F. Fan and A. J. Bard, *J. Phys. Chem. B*, 1997, **101**, 5707-5711.
17. S. Gawęda, R. Kowalik, P. Kwolek, W. Macyk, J. Mech, M. Oszajca, A. Podborska and K. Szaciłowski, *Isr. J. Chem.*, 2011, **51**, 36-55.
18. S. Gawęda, G. Stochel and K. Szaciłowski, *J. Phys. Chem. C*, 2008, **112**, 19131-19141.
19. S. Gawęda, G. Stochel and K. Szaciłowski, *Chem. Asian J.*, 2007, **2**, 580-590.
20. K. Szaciłowski, W. Macyk and G. Stochel, *J. Mater. Chem.*, 2006, **16**, 4603-4611.
21. K. Szaciłowski and W. Macyk, *Solid State Electron.*, 2006, **50**, 1649-1655.
22. K. Szaciłowski, W. Macyk and G. Stochel, *J. Am. Chem. Soc.*, 2006, **128**, 4550-4551.
23. M. Hebda, G. Stochel, K. Szaciłowski and W. Macyk, *J. Phys. Chem. B*, 2006, **110**, 15275-15283.
24. K. Szaciłowski, W. Macyk, M. Hebda and G. Stochel, *ChemPhysChem*, 2006, **7**, 2384-2391.
25. J. Mech, K. Mech and K. Szaciłowski, *J. Mater. Chem. C*, 2015, **3**, 4148-4155.
26. Y. Di Iorio, H. B. Rodríguez, E. San Román and M. A. Grela, *J. Phys. Chem. C*, 2010, **114**, 11515-11521.

27. Y. Di Iorio, R. Parra, K. Szaciłowski and M. A. Grela, *New J. Chem*, 2013, **37**, 969-976.

28. W. Macyk, G. Stochel and K. Szaciłowski, *Chem. Eur. J.*, 2007, **13**, 5676-5687.

29. K. Szaciłowski, W. Macyk and G. Stochel, *J. Mater. Chem.*, 2006, **16**, 4603–4611.

30. M. Oszajca, K. L. McCall, N. Robertson and K. Szaciłowski, *J. Phys. Chem. C*, 2011, **115**, 12187-12195.

31. M. Warzecha, M. Oszajca, K. Pilarczyk and K. Szaciłowski, *Chem. Commun.*, 2015, **51**, 3559-3561.

32. J. Kuncewicz, P. Ząbek, K. Kruczała, K. Szaciłowski and W. Macyk, *J. Phys. Chem. C*, 2012, **116**, 21762-21770.

33. K. Lewandowska, A. Podborska, P. Kwolek, T.-D. Kim, K.-S. Lee and K. Szaciłowski, *Appl. Surf. Sci.*, 2014, **319**, 285-290.

34. R. Beránek and H. Kisch, *Angew. Chem. Int. Ed.*, 2008, **47**, 1320-1322.

35. R. Memming, *Semiconductor electrochemistry*, first edn., Wiley-VCH, Weinheim, 2001.

36. P. Wardman, *J. Phys. Chem. Ref. Data*, 1989, **18**, 1637-1755.

37. D. T. Sawyer and J. S. Valentine, *Acc. Chem. Res.*, 1981, **14**, 393-400.

38. A. J. Bard, M. Stratmann and S. Licht, *Encyclopedia of Electrochemistry, Semiconductor Electrodes and Photoelectrochemistry*, Wiley, 2002.

39. M. G. Walter, E. L. Warren, J. R. McKone, S. W. Boettcher, Q. Mi, E. A. Santori and N. S. Lewis, *Chem. Rev.*, 2010, **110**, 6446-6473.

40. M. X. Tan, P. E. Laibinis, S. T. Nguyen, J. M. Kesselman, C. E. Stanton and N. S. Lewis, *Prog. Inorg. Chem.*, 1994, **41**, 21-144.

41. R. van de Krol and M. Grätzel, *Photoelectrochemical Hydrogen Production*, Springer, 2011.

42. W. J. Yin, S. H. Wei, M. M. Al-Jassim, J. Turner and Y. Yan, *Phys. Rev. B*, 2011, **83**.

43. G. Hodes, I. D. J. Howell and L. M. Peter, *J. Electrochem. Soc.*, 1992, **139**, 3136-3140.

44. J. Kuncewicz, P. Ząbek, K. Kruczała, K. Szaciłowski and W. Macyk, *J. Phys. Chem. C*, 2012, **116**, 21762-21770.

45. X. Chen, S. Yeganeh, L. Qin, S. Li, C. Xue, A. B. Braunschweig, G. C. Schatz, M. A. Ratner and C. A. Mirkin, *Nano Lett.*, 2009, **12**, 3974-3979.

46. O. V. Prezhdo, W. R. Duncan and V. V. Prezhdo, *Progr. Surf. Sci.*, 2009, **84**, 30-68.

47. C. Creutz, B. S. Brunschwig and N. Sutin, *J. Phys. Chem. B*, 2005, **109**, 10251-10260.

48. C. Creutz, B. S. Brunschwig and N. Sutin, *Chem. Phys.*, 2006, **324**, 244-258.

49. D. M. Adams, L. Brus, C. E. D. Chidsey, S. Creager, C. Creutz, C. R. Kagan, P. V. Kamat, M. Lieberman, S. Lindsay, R. A. Marcus, R. M. Metzger, M. E. Michel-Beyerle, J. R. Miller, M. D. Newton, D. R. Rolison, O. Sankey, K. S. Schanze, J. Yardley and X. Zhu, *J. Phys. Chem. B*, 2003, **107**, 6668-6697.

50. C. Creutz, B. S. Brunschwig and N. Sutin, *J. Phys. Chem. B*, 2006, **110**, 25181-25190.

51. T. Sakata, K. Hashimoto and M. Hiramoto, *J. Phys. Chem.*, 1990, **94**, 3040-3045.

52. O. Kitao, *J. Phys. Chem. C*, 2007, **111**, 15889-15902.

53. P. Kwolek, M. Oszajca and K. Szaciłowski, *Coord. Chem . Rev.*, 2012, **56**, 1706-1731.

54. W. Macyk, K. Szaciłowski, G. Stochel, M. Buchalska, J. Kuncewicz and P. Łabuz, *Coord. Chem. Rev.*, 2010, **254**, 2687-2701.

55. M. Oszajca, P. Kwolek, J. Mech and K. Szaciłowski, *Curr. Phys. Chem.*, 2011, **1**, 242-260.

56. L. G. C. Rego and V. S. Batista, *J. Am. Chem. Soc.*, 2003, **125**, 7989-7997.

57. S. G. Abuabara, L. G. C. Rego and V. S. Batista, *J. Am. Chem. Soc.*, 2005, **127**, 18234-18242.

58.   O. V. Prezhdo, W. R. Duncan and V. V. Prezhdo, *Acc. Chem. Res.*, 2008, **41**, 339-348.

59.   W. R. Duncan and O. V. Prezhdo, *Annu. Rev. Phys. Chem.*, 2007, **58**, 143-184.

60.   S. Ardo and G. J. Meyer, *Chem. Soc. Rev.*, 2009, **38**, 115-164.

61.   W. R. Duncan, W. M. Stier and O. V. Prezhdo, *J. Am. Chem. Soc.*, 2005, **127**, 7941-7951.

62.   T. Rajh, L. X. Chen, K. Lukas, T. Liu, M. C. Thurnauer and D. M. Tiede, *J. Phys. Chem. B*, 2002, **106**, 10543-10552.

63.   A. E. Regazzoni, P. Mandelbaum, M. Matsuyoshi, S. Schiller, S. A. Bilmes and M. A. Blesa, *Langmuir*, 1998, **14**, 868-874.

64.   K. Szaciłowski and W. Macyk, *Chimia*, 2007, **61**, 831-834.

65.   M. Long, R. Beránek, W. Cai and H. Kisch, *Electrochim. Acta*, 2008, **53**, 4621-4626.

66.   G. Agostinelli and E. D. Dunlop, *Thin Solid Films*, 2003, **431-432**, 448-452.

67.   K. M. Nam, H. S. Park, H. C. Lee, B. H. Meekins, Kevin C. Leonard and A. J. Bard, *J. Phys. Chem. Lett.*, 2013, **4**, 2707-2710.

68.   J. Y. Zheng, G. Song, C. W. Kim and Y. S. Kang, *Electrochim. Acta*, 2012, **69**, 340-344.

69.   B. Daly, J. Ling and A. P. de Silva, *Chem. Soc. Rev.*, 2015, **44**, 4203-4211.

70.   J. Ling, B. Daly, V. A. D. Silverson and A. P. de Silva, *Chem. Commun.*, 2015, **51**, 8403-8409.

71.   E. Bishop, *Indicators*, Pergamon Press, Oxford, 1972.

72.   A. B. Richard, A. P. de Silva, H. Q. N. Gunaratne, P. L. M. Lynch, G. E. M. Maquire and K. R. A. S. Sandanayake, *Chem. Soc. Rev.*, 1992, **21**, 187-195.

73.   A. P. de Silva, T. P. Vance, M. E. S. West and G. D. Wright, *Org. Biomol. Chem.*, 2008, **6**, 2468-2481.

74.   A. P. de Silva, H. Q. N. Gunaratne, P. L. M. Lynch, A. J. Patty and G. L. Spence, *J. Chem. Soc., Perkin Trans. 2*, 1993, **10**, 1611-1616.

75.   S. Uchiyama, T. Santa and K. Imai, *Analyst*, 2000, **125**, 1839-1845.

76.   Y. Q. Gao and R. A. Marcus, *J. Phys. Chem. A*, 2002, **2002**, 1956-1960.

77.   T. Kowalczyk, Z. Lin and T. V. Voorhis, *J. Phys. Chem. A*, 2010, **114**, 10427-10434.

78.   P. Batat, G. Vives, R. Bofinger, R.-W. Chang, B. Kauffmann, R. Oda, G. Jonusauskas and N. D. McClenaghan, *Photochem. Photobiol. Sci.*, 2012, **11**, 1666-1674.

79.   H. Lee, R. D. Hancock and H.-S. Lee, *J. Phys. Chem. A*, 2013, **117**, 13345-13355.

80.   H. Su, X. Chen and W. Fang, *Anal. Chem.*, 2014, **86**, 891-899.

81.   R. Sun, X.-D. Liu, Z. Xun, J.-M. Lu, Y.-J. Xu and J.-F. Ge, *Sensors and Actuators B*, 2014, **201**, 426-432.

82.   Y. Xu, Z. Jiang, Y. Xiao, F.-Z. Bi, J.-Y. Miao and B.-X. Zhao, *Anal. Chim. Acta*, 2014, **820**, 146-151.

83.   Q. Wang and Xueye, *J. Phys. Org. Chem.*, 2014, **27**, 546-554.

84.   M. J. Frisch, G. W. Trucks, H. B. Schlegel, G. E. Scuseria, M. A. Robb, J. R. Cheeseman, G. Scalmani, V. Barone, B. Mennucci, G. A. Petersson, H. Nakatsuji, M. Caricato, X. Li, H. P. Hratchian, A. F. Izmaylov, J. Bloino, G. Zheng, J. L. Sonnenberg, M. Hada, M. Ehara, K. Toyota, R. Fukuda, J. Hasegawa, M. Ishida, T. Nakajima, Y. Honda, O. Kitao, H. Nakai, T. Vreven, J. A. Montgomery Jr., J. E. Peralta, F. Ogliaro, M. Bearpark, J. J. Heyd, E. Brothers, K. N. Kudin, V. N. Staroverov, R. Kobayashi, J. Normand, K. Raghavachari, A. Rendell, J. C. Burant, S. S. Iyengar, J. Tomasi, M. Cossi, N. Rega, J. M. Millam, M. Klene, J. E. Knox, J. B. Cross, V. Bakken, C. Adamo, J. Jaramillo, R. Gomperts, R. E. Stratmann, O. Yazyev, A. J. Austin, R. Cammi, C. Pomelli, J. W. Ochterski, R. L. Martin, K. Morokuma, V. G. Zakrzewski, G. A. Voth, P. Salvador, J. J. Dannenberg, S. Dapprich, A. D. Daniels,

O. Farkas, J. B. Foresman, J. V. Ortiz, J. Cioslowski and D. J. Fox, *Gaussian 09, Rev. A.02*, Gaussian, Inc., Wallingford CT, 2009.

85. www.probes.com.
86. Z. R. Grabowski and J. Dobkowski, *Pure & Appl. Chem.*, 1983, **55**, 245-253.
87. Y. Moroi, *Micelles. Theoretical and Applied Aspects*, Springer, New York, 1992.
88. F. M. Harold, *The Vital Force - A Study of Bioenergetics*, Freeman, New York, 1986.
89. R. A. Bissell, A. J. Bryan, A. P. de Silva and C. P. McCoy, *J. Chem. Soc. Chem. Commun.*, 1994, 405-407.
90. S. Uchiyama, K. Iwai and A. P. de Silva, *Angew. Chem. Int. Ed.*, 2008, **47**, 4667-4669.
91. M. D. P. de Costa, A. P. de Silva and S. T. Pathirana, *Canad. J. Chem.*, 1987, **69**, 1416-1419.
92. M. S. Fernandez and P. Fromherz, *J. Phys. Chem.*, 1977, **81**, 1755-1761.
93. B. Valeur, *Molecular fluorescence. Principles and applications*, Wiley-VCH, Weinheim, 2002.
94. S. Uchiyama, E. Fukatsu, G. D. McClean and A. P. de Silva, *Angew. Chem. Int. Ed.*, 2015, **55**, 768-771.
95. R. M. Izatt, R. E. Terry, D. P. Nelson, Y. Chan, D. J. Eatough, J. S. Bradshaw, L. D. Hansen and J. J. Christensen, *J. Am. Chem .Soc.*, 1976, **98**, 7626-7630.
96. A. P. de Silva and K. R. A. S. Sandanayake, *Tetrahedron Lett.*, 1991, **32**, 421-424.
97. C. Gota, S. Uchiyama, T. Yoshihara, S. Tobita and T. Ohwada, *J. Phys. Chem. B*, 2008, **112**, 2829-2836.
98. R. Y. Tsien and M. Poenie, *Trends Biochem. Sci.*, 1986, **11**, 450-455.
99. J. Lechleiter, S. Girard, E. Peralta and D. Clapham, *Science*, 1991, **252**, 123-126.
100. X. Qian, Y. Xiao, Y. Xu, X. Guo, J. Qian and W. Zhu, *Chem. Commun.*, 2010, **46**, 6418-6436.
101. R. A. Schultz, B. D. White, D. M. Dishong, K. A. Arnold and G. W. Gokel, *J.Am. Chem. Soc.*, 1985, **107**, 6659-6668.
102. J. K. Tusa and H. He, *J. Mater. Chem.*, 2005, **15**, 2640-2647.
103. www.optimedical.com.
104. A. P. Malvino and J. A. Brown, *Digital Computer Electronics*, Glencoe, Lake Forest, 1993.
105. A. L. Sedra and K. C. Smith, *Microelectronic Circuits 5th Ed.*, Oxford University Press, Oxford, 2003.
106. A. P. de Silva, H. Q. N. Gunaratne and C. P. McCoy, *Nature*, 1993, **364**, 42-44.
107. S. Gawęda, A. Podborska, W. Macyk and K. Szaciłowski, *Nanoscale*, 2009, **1**, 299-316.
108. S. Gawęda, G. Stochel and K. Szaciłowski, *J. Phys. Chem C*, 2008, **112**, 19131-19141.
109. M. Bendikov, F. Wudl and D. F. Perepichka, *Chem. Rev.*, 2004, **104**, 4891-4945.
110. H. Ishii, K. Sugiyama, E. Ito and K. Seki, *Adv. Mater.*, 1999, **11**, 605-625.
111. S. Gawęda, A. Podborska, W. Macyk and K. Szaciłowski, *Nanoscale*, 2009, **1**, 299-316.
112. A. L. Linsebigler, G. Lu and J. T. Yates Jr., *Chem. Rev.*, 1995, **95**, 735-758.
113. A. Fujishima, X. Zhang and D. A. Tryk, *Surf. Sci. Reports*, 2008, **63**, 515-582.
114. A. Podborska and K. Szaciłowski, *Aust. J. Chem.*, 2010, **63**, 165-168.
115. A. Maharjan, K. Pemasiri, P. Kumar, A. Wade, L. M. Smith, H. E. Jackson, J. M. Yarrison-Rice, A. Kogan, S. Paiman, Q. Gao, H. H. Tan and C. Jagadish, *Appl. Phys. Lett.*, 2009, **94**, 193115.
116. F. Yang, K. Huang, S. Ni, Q. Wang and D. He, *Nanoscale Res. Lett.*, 2010, **5**, 416-419.

117. X. Fang, Y. Bando, M. Liao, U. K. Gautam, C. Zhi, B. Dierre, B. Liu, T. Zhai, T. Sekiguchi, Y. Koide and D. Golberg, *Adv. Mater.*, 2009, **21**, 2034-2039.
118. T. Zhai, X. Fang, L. Li, Y. Bando and D. Goldberg, *Nanoscale*, 2010, **2**, 168-187.
119. J. Mech, R. Kowalik, A. Podborska, P. Kwolek and K. Szaciłowski, *Aust. J. Chem.*, 2010, **63**, 1330-1333.
120. A. P. de Silva, H. Q. N. Gunaratne and G. E. M. Maguire, *J. Chem. Soc. Chem. Commun.*, 1994, 1213-1214.
121. A. P. de Silva, H. Q. N. Gunaratne and C. P. McCoy, *J. Am. Chem. Soc.*, 1997, **119**, 7891-7892.
122. A. P. de Silva, I. M. Dixon, H. Q. N. Gunaratne, T. Gunnlaugsson, P. R. S. Maxwell and T. E. Rice, *J. Am. Chem. Soc.*, 1999, **121**, 1393-1394.
123. A. P. de Silva and N. D. McClenaghan, *J. Am. Chem. Soc.*, 2000, **122**, 3965-3966.
124. S. Uchiyama, N. Kawai, A. P. de Silva and K. Iwai, *J. Am. Chem. Soc.*, 2004, **126**, 3032-3033.
125. G. J. Brown, A. P. de Silva and S. Pagliari, *Chem. Commun.*, 2002, 2461-2463.
126. D. C. Magri, G. J. Brown, G. D. McClean and A. P. de Silva, *J. Am. Chem. Soc.*, 2006, **128**, 4950-4951.
127. J. Łukasiewicz, *Aristotle's Syllogistic from the Standpoint of Modern Formal Logic*, Claredon Press, Oxford, 1951.
128. L. Goble, *The Blackwell Guide to Philosophical Logic*, Wiley-Blackwell, Hoboken, 2001.
129. J. Łukasiewicz, *Selected Works*, North-Holland, Amsterdam, 1970.
130. M. Fisch and A. Turquette, *T.C.S. Peirce Soc.*, 1966, **2**, 71-85.
131. M. Elati, P. Neuvial, M. Bolotin-Fukuhara, E. Barillot, F. Radvanyi and C. Rouveirol, *Bioinformatics*, 2007, **23**, 2407-2414.
132. M. K. Morris, J. Saez-Rodriguez, P. K. Sorger and D. A. Lauffenburger, *Biochemistry*, 2010, **49**, 3216-3224.
133. I. G. A. de Rojas, *Logical and Linguistic Problems of Social Communication with Aymara People*, International Development Research Centre (IDRC), Ottawa, 1984.
134. J. Miriel and F. Fermanel, *Appl. Energ.*, 2001, **68**, 229-247.
135. A. Glaser, *History of binary and other nondecimal numeration*, Tomash Publishers, Los Angeles, 1971.
136. Y. Jin, H. He and Y. Lü, *Sci. China Ser. F*, 2003, **46**, 145-150.
137. N. P. Brousentsov, S. P. Maslov, J. Ramil Alvarez and E. A. Zhogolev, *Development of ternary computers at Moscow State University*, http://www.computer-museum.ru/english/setun.htm, Accessed 2010-03-26, 2010.
138. A. Stakhov, *Comput. J.*, 2002, **45**, 221-236.
139. M. Morisue, J. Endo, T. Morooka, N. Shimizu and M. Sakamoto, *28th Int. Sym. Multi Valued Logic*, 1998, 19-24.
140. J. Natarajan, M. Coles and M. Cebollero, *Pro T-SQL Programmer's Guide*, Apress, New York, 2015.
141. J. Liang, L. Chen, J. Han and F. Lombardi, *IEEE Trans. Nanotech.*, 2014, **13**, 695-708.
142. I. L. Bajec, N. Zimic and M. Mraz, *Nanotechnology*, 2006, **17**, 1937-1942.
143. P. V. Saidutt, V. Srinivas, P. S. Phaneendra and N. M. Muthukrishnan, 2012 Asia Pacific Conference on Postgraduate Research in Microelectronics and Electronics (PrimeAsia), 2012.
144. S. Liu, C. Li, J. Wu and Y. Liu, *Opt. Lett.*, 1989, **14**, 713-715.
145. P. Remón, R. Ferreira, J. M. Montenegro, R. Suau, E. Pérez-Inestrosa and U. Pischel, *ChemPhysChem*, 2009, **10**, 2004-2007.

146. S. Shepard, *RDIF: Radio Frequency Identification*, McGraw-Hill, New York, 2005.

147. K. L. Michael, L. C. Taylor, S. L. Schultz and D. R. Walt, *Anal. Chem.*, 1998, **70**, 1242-1248.

148. Smith Kline Beecham Corp. *US Pat.* 6,210,900 B1, 3 April 2001.

149. A. P. de Silva, M. R. James, B. O. F. McKinney, D. A. Pears and S. M. Weir, *Nat. Mater.*, 2006, **5**, 787-789.

150. B. Hayes, *Am. Sci.*, 2001, **89**, 490-494.

151. P. L. Gentili, *J. Intell. Fuzzy Syst.*, 2014, **27**, 2137-2151.

152. P. L. Gentili, *RSC Adv.*, 2013, **3**, 25523-25549.

153. L. A. Zadeh, *Inform. Control*, 1965, **8**, 338–353.

154. M. Bergmann, *An Introduction to Many-Valued and Fuzzy Logic: Semantics, Algebras, and Derivation Systems*, Cambridge University Press, Cambridge, 2008.

155. E. H. Mamdani and S. Assilian, *Int. J. Human-Computer Studies*, 1999, **51**, 135-147.

156. L. A. Bryan and E. A. Bryan, *Programmable controllers: theory and implementation*, Industrial Text Company, Marietta, 1997.

157. P. L. Gentili, V. Horvath, V. K. Vanag and I. R. Epstein, *Int. J. Uncov. Comput.*, 2012, **8**, 177-192.

158. P. L. Gentili, *J. Phys. Chem. A*, 2008, **112**, 11992-11997.

159. P. L. Gentili, *Chem. Phys.*, 2007, **336**, 64-73.

160. P. L. Gentili, *Phys. Chem. Chem. Phys*, 2011, **13**, 20335-20344.

161. P. L. Gentili, *Dyes Pigments*, 2014, **110**, 235-248.

162. P. L. Gentili, *ChemPhysChem*, 2011, **12**, 739-745.

163. R. Deaton and M. Garzon, *Soft Comput.*, 2001, **5**, 2-9.

164. R. M. Zadegan, M. D. E. Jepsen, L. L. Hildebrandt, V. Birkedal and J. Kjems, *Small*, 2015, **11**, 1811-1817.

165. V. N. Huynh, T. B. Ho and Y. Nakamori, *Int. J. Approx. Reason.*, 2002, **30**, 203-223.

166. J. S. R. Jang, *IEEE T. Syst. Man Cyb.*, 1993, **23**, 665-684.

167. J. S. R. Jang and C. T. Sun, *Proc. IEEE*, 1995, **83**, 378-405.

168. http://top500.org/.

169. S. Song, K. D. Miller and L. F. Abbott, *Nat. Neurosci.*, 2000, **3**, 919-926.

170. N. Caporale and Y. Dan, *Annu. Rev. Neurosci.*, 2008, **31**, 25-46.

171. D. E. Feldman, *Neuron*, 2012, **75**, 556-571.

172. S. J. Martin, P. D. Grimwood and R. G. M. Morris, *Annu. Rev. Neurosci.*, 2000, **23**, 649-711.

173. D. George and B. Jaros, *Numenta Inc. Report*, 2007.

174. J. Hawkins and D. George, *Numenta Inc. Report*, 2006.

175. B. Warneke, M. Last, B. Liebowitz and K. S. J. Pister, *Computer*, 1997, **34**, 2-9.

176. J. R. Link and M. J. Sailor, *Proc. Natl. Acad. Sci.*, 2003, **100**, 10607-10610.

177. M. J. Sailor and J. R. Link, *Chem. Commun.*, 2005, 1375-1383.

178. E. Katz and I. Willner, *Angew. Chem. Int. Ed.*, 2004, **43**, 6042-6108.

179. E. Katz, I. Willner and J. Wang, *Electroanalysis*, 2004, **16**, 19-43.

180. A. Burns, H. Ow and U. Wiesner, *Chem. Soc. Rev.*, 2006, **35**, 1028-1042.

181. A. Burns, P. Sengupta, T. Zedayko, B. Baird and U. Wiesner, *Small*, 2006, **2**, 723-726.

182. R. Gill, M. Zayats and I. Willner, *Angew. Chem. Int. Ed.*, 2008, **47**, 7602-7625.

183. S. Uchiyama, G. D. McClean, K. Iwai and A. P. de Silva, *J. Am. Chem. Soc.*, 2005, **127**, 8920-8921.

184. A. P. de Silva, C. M. Dobbin, T. P. Vance and B. Wannalerse, *Chem. Commun.*, 2009, 1386-1388.

185. P. Pallavicini, Y. A. Diaz-Fernandez and L. Pasotti, *Coord. Chem. Rev.*, 2009, **253**, 2226-2240.
186. V. Erokhin, T. Berzina, A. Smerieri, P. Camorani, S. Erokhina and M. P. Fontana, *Nano Commun. Networks*, 2010, **1**, 108-117.
187. V. Erokhin, T. Berzina, P. Camorani, A. Smerieri, D. Vavoulis, J. Feng and M. P. Fontana, *BioNanoSci.*, 2011, **1**, 24-30.
188. V. Erokhin, T. Berzina, P. Camorani and M. P. Fontana, *J. Phys. Condens. Matter*, 2007, **19**, 205111.
189. T. Berzina, A. Smerieri, M. Barnabó, A. Pucci, G. Ruggieri, V. Erokhin and M. P. Fontana, *J. Appl. Phys.*, 2009, **105**, 124515.
190. T. Ohno, T. Hasegawa, T. Tsuruoka, K. Terabe, J. K. Gimzewski and M. Aono, *Nat. Mater.*, 2010, **10**, 591-595.
191. K. Kim, C.-L. Chen, Q. Truong, A. M. Shen and Y. Chen, *Adv. Mater.*, 2013, **25**, 1693-1698.
192. O. Bichler, W. Zhao, F. Alibart, S. Pleutin, D. Vuillaume and C. Gamrat, *IEEE Trans. Electron Dev.*, 2010, **57**, 3115-3122.
193. W. Gerstner and W. M. Kistler, *Biol. Cybern.*, 2002, **87**, 404-415.
194. V. Datsyuk, M. Kalyva, K. Papagelis, J. Parthenios, D. Tasis, A. Siokou, I. Kallitsis and C. Galiotis, *Carbon*, 2008, **46**, 833-840.
195. G. Q. Bi and M. M. Poo, *J. Neurosci.*, 1998, **18**, 10464-10472.
196. R. Legenstein, D. Pecevski and W. Maass, *PLoS Comput. Biol.*, 2008, **4**, e10000180.
197. I. R. Fiete, W. Senn, C. Z. H. Wang and R. H. R. Hahnloser, *Neuron*, 2010, **65**, 563-576.
198. C. Rutherglen and P. Burke, *Nano Lett.*, 2007, **7**, 3296-3299.
199. V. Bruce, P. R. Green and M. A. Georgeson, *Visual Perception 4th Ed.*, Psychology Press, Hove, 2003.
200. O. F. Lazareva, T. Shimizu and E. A. Wasseman, *How animals see the world*, Oxford University Press, Oxford, 2012.
201. H. S. Hock and D. F. Nichols, *Atten. Percept. Psychophys.*, 2013, **75**, 726-737.
202. L. G. Shapiro and G. C. Stockman, *Computer vision*, Prentice-Hall, Upper Saddle River, 2001.
203. J. J. Tabor, H. M. Salis, Z. B. Simpson, A. A. Chevalier, A. Levskaya, E. M. Marcotte, C. A. Voigt and A. D. Ellington, *Cell*, 2009, **137**, 1272-1281.
204. S. M. Chirieleison, P. B. Allen, Z. B. Simpson, A. D. Ellington and X. Chen, *Nature Chem.*, 2013, **5**, 1000-1005.
205. J. Ling, G. Naren, J. Kelly, T. S. Moody and A. P. de Silva, *J. Am. Chem. Soc.*, 2015, **137**, 3763-3766.
206. J. L. Dektar and N. P. Hacker, *J. Am. Chem. Soc.*, 1990, **112**, 6004-6015.
207. L. M. Daffy, A. P. de Silva, H. Q. N. Gunaratne, C. Huber, P. L. M. Lynch, T. Werner and O. S. Wolfbeis, *Chem. Eur. J.*, 1998, **4**.
208. J. Ling, G. Naren, J. Kelly, D. B. Fox and A. P. de Silva, *Chem. Sci.*, 2015, **6**, 4472-4478.
209. F. Pina, M. J. Melo, M. Maestri, P. Passanit and V. Balzani, *J. Am. Chem. Soc.*, 2000, **122**, 4496-4498.
210. S. Silvi, E. C. Constable, C. E. Housecroft, J. E. Beves, E. L. Dunphy, M. Tomasulo, F. M. Raymo and A. Credi, *Chem. Eur. J.*, 2009, **15**, 178-185.
211. S. Silvi, E. C. Constable, C. E. Housecroft, J. E. Beves, E. L. Dunphy, M. Tomasulo, F. M. Raymo and A. Credi, *Chem. Commun.*, 2009, 1484-1486.
212. M. P. O'Neil, M. P. Niemczyk, W. A. Svec, D. Gosztola, G. L. Gaines and M. R. Wasielewski, *Science*, 1992, **257**, 63-65.

213.   V. F. Pais, P. Remón, D. Collado, J. Andréasson, E. Pérez-Inestrosa and U. Pischel, *Org. Lett.*, 2011, **13**, 5572-5575.
214.   A. P. de Silva, H. Q. N. Gunaratne and C. P. McCoy, *Chem. Commun.*, 1996, 2399-2400.
215.   H. Nouri, C. Cadiou, L. M. Lawson-Daku, A. Hauser, S. Chevreux, I. Déchamps-Olivier, F. Lachaud, R. Ternane, M. Trabelsi-Ayadi, F. Chuburu and G. Lemercier, *Dalton Trans.*, 2013, **42**, 12157-12164.
216.   J. F. Callan, A. P. de Silva, J. Ferguson, A. J. M. Huxley and A. M. O'Brien, *Tetrahedron*, 2004, **60**, 11125-11131.